Quantifying the Role of Urbanization on Airflow Perturbations and Dunefield Evolution

Alexander B. Smith*[1], Derek W. T. Jackson[1], J. Andrew G. Cooper[1,2], and L. Hernández-Calvento[3]

1. School of Geography and Environmental Science, Ulster University, Coleraine, BT52 1SA, Northern Ireland, United Kingdom.
2. Geological Sciences, School of Agricultural, Earth and Environmental Sciences, University of KwaZulu-Natal, Westville Campus, Private Bag X54001, South Africa
3. Instituto de Oceanografía y Cambio Global, IOCAG. Universidad de Las Palmas de Gran Canaria, ULPGC, Parque Científico-Tecnológico de Taliarte, 35214 Telde, Las Palmas, Spain.

Abstract:

Rapid urban development has been widespread in many arid regions of the world during the Anthropocene. Such development has the potential to affect, and be affected by, local and regional dunefield dynamics. While urban design often includes consideration of the wind regime, the potential impact of construction on the surrounding environment is seldom considered and remains poorly understood. In this study regional airflow modelling during successive stages of urbanization at Maspalomas, Gran Canaria, Spain, indicates significant and progressive flow perturbations that have altered the adjacent dunefield. Significant modifications to the boundary layer velocity, mean wind directionality, turbulence intensity, and sediment flux potential are attributed to the extension of the evolving urban geometry into the internal boundary layer (IBL).

Two distinct process/response zones were identified: (1) the urban shadow zone where widespread dune stabilization is attributed to the sheltering effect of the urban area on surface wind velocity; and (2) the acceleration zone where airflow is deflected away from the urbanized area, causing an increase in sediment transport potential and surface erosion. Consistent coherent turbulent structures were identified at landform and dunefield scales: counter-rotating vortices develop in the lee-side flow of dune crests and shedding off the buildings on the downwind edge of the urban area. This study illustrates the direct geomorphic impact of urbanization on aeolian dunefield dynamics, a relationship that has received little previous attention. The study provides a template for investigations of the potential impact of urbanization in arid zones.

Keywords: Aeolian dynamics, Anthropogenic impact, Turbulence, Coherent flow structures, CFD modelling.

1. Introduction

Although many natural and anthropogenic factors influence dunefield mobility the interaction between urbanization and physical processes has been little studied [Nordstrom, 1994; Jackson and Nordstrom, 2011]. The proliferation of urbanization in arid zones during the past 50 years makes the understanding between human developments and dunefields, a unique issue of the Anthropocene. Large scale human development of dune environments has caused a fundamental alteration from a natural state (see review by [Nordstrom, 1994]). Buildings located adjacent to or within dunefields act as hard impervious structures that extend into the Internal Boundary Layer (IBL) and impact aeolian dynamics and the regional geomorphology [Nordstrom and Mcluskey, 1984; Gundlach and Siah, 1987; Nordstrom and Jackson, 1998]. These small-scale, empirical studies found that buildings invoke airflow perturbations including steering and changes in wind velocity, and generate secondary flow patterns (e.g. separation and recirculation cells). These perturbed flow dynamics alter sediment transport patterns both up- and downwind of buildings [Nordstrom and Mcluskey, 1984; Gundlach and Siah, 1987; Nordstrom and Jackson, 1998]. With widespread urban development in arid regions, the relationship between dunefield dynamics and urban infrastructure become important considerations. A meso-scale perspective is needed to provide an understanding of the complexity of regional airflow modified by human development. Given the difficulties in measuring this influence, numerical models can provide a broader understanding of impacts at landform and landscape scales.

Computational Fluid Dynamics (CFD) has been an increasingly utilized tool for research in aeolian geomorphology [see review by Smyth, 2016]. It enables the identification of topographically modified flow including characteristic airflow conditions, complex turbulent structures [Bauer et al., 2013; Jackson et al., 2013a], and sediment transport patterns [Lynch et al., 2013; 2016]. Previous CFD studies have identified topographically modified controls on primary and complex secondary airflow dynamics but none have addressed the impact of human development (e.g. urbanization) on airflow and dune dynamics. Previous urban CFD studies have focused on a wide range of issues including airflow and pollutant dispersion [Murakami et al., 1999; Kim et al., 2003; Pullen et al., 2005; Hanna et al., 2006; Sabatino et al., 2007; Bai and Park, 2009], building pressures [Richards and Hoxey, 2012], and human comfort and safety [Blocken et al, 2012; Fadl and Karadelis, 2013]. While these studies have addressed a wide range of topics they do provide a useful list of methods addressing model selection, initial boundary conditions, and urban geometries that can be applied across a range of disciplines.

Hernández-Calvento et al. [2014] provided the first study of its kind in implementing an urban airflow model in a geomorphological context. The authors simulated flow conditions around the Maspalomas dunefield, Gran Canaria (Spain) using a simplified numerical model based on a logarithmic wind profile to analyse perturbed flow velocity and directionality for pre- and post-urbanization of an elevated paleo-alluvial terrace that extends down through the central section of the dunefield. The model surface was tiered using constant heights for dune topography at 7 m above mean sea level (MSL), the terrace surface prior to urbanization at 20 m above MSL, and the terrace surface following urbanization at 40 m above MSL. The grid dimensions were 5,000 (x) x 5,000 (y) x 50 (z) with a cell size of 50 m. With this simplified numerical model and idealized terrain surface, significant perturbations to velocity and steering were identified in relation to simulated ENE wind conditions. This study implements CFD modelling, on actual dune topography acquired from LiDAR, and detailed 3D building geometries across the terrace at Maspalomas through time in order to identify the intensity of regional flow modification at decadal scales.

The main objectives of this study are therefore to: (1) identify the regional airflow perturbations that can be directly attributable to urbanization during various stages of urban development; (2) describe the geomorphic evolution of the dunefield following each phase of development; (3) analyse any climatic variability that may have contributed to modified dune activity through these time periods; (4) determine sediment transport potential and pathways pre- and post- urbanization; and (5) examine the role of coherent turbulent flow structures that develop across the dune and urban model surfaces. The study provides a template for future investigations of actual and potential impacts of urbanization on arid zone dunes.

2. Study Site

Maspalomas (27°44’24.73” N and 15°34’26.19” W) is a 3.6 km² arid transgressive dune system located on the southern coast of Gran Canaria, Spain (Fig. 1a,c). The competent wind regime is bi-modal, characterised by low frequency W storm events and high frequency prevailing NE trade winds (Fig. 1b). Given the magnitude and frequency of the trade winds, the dunes migrate from the source area at Playa del Inglés towards the SW to the terminus at

Playa de Maspalomas (Fig. 1a). The dunefield is comprised of highly mobile discrete barchans, barchanoid dune ridges, small parabolics, nebkhas, and sand sheets.

2.1. Physical Setting

A narrow offshore shelf, adjacent to Playa del Inglés, provides the majority of sediment input into the littoral system [Bouzas et al., 2013]. After the sediment moves through the dunefield, it is redeposited on the offshore shelf at Playa de Maspalomas, the dunefield acting as a terrestrial sediment conduit. Despite a substantial volume (63.1 x 10^6 m^3) of sediment located on the shelf, the system as a whole is in decline as the littoral deposition of sediment from the NE does not keep pace with the loss of sediment in the SE [Bouzas et al., 2013]. The updrift shoreline, at Playa del Inglés, has remained relatively stable in recent decades providing consistent sediment input into the dune system [Fontan et al., 2012]. The dunefield contains 18.6 x 10^6 m^3 of sediment [Alcántara-Carrió and Fontán, 2009], of which 14.1 x 10^6 m^3 are available for transport [Vallejo et al., 2009]. Hernández et al. [2007] identified a sediment deficit within the dunefield as the overall heights of the dunes and accumulation ridges have decreased and the area of deflation down to the basement alluvium layer has increased over the past 40 years.

2.2. Anthropogenic Development

Intense urbanization has occurred across the elevated paleo-alluvial terrace that extends through the central section of the dunefield, between the mid-1960s until the late 1990s. Prior to the 1960s, this area was primarily agricultural with climbing dunes able to bypass the terrace before continuing migration unimpeded towards the W [Hernández Calvento, 2006] (Fig. 2a). By 2006, the terrace was completely urbanized (Fig. 2b). The margins of the dunefields have also been affected by building of a golf course, apartments, resorts, hotels and commercial centres. This has led to both a reduction in the aerial extent of the dune field and directly modified the regional sediment pathways and airflow dynamics. Coinciding with urbanization, the NW section of the dunefield has become widely stabilized due to the reduction of wind energy, lack of sediment influx, and large scale colonization of vegetation in this area [Hernández et al., 2007]. In contrast, the active section of the dunefield has experienced increased erosion as the lowering of the dune topography and the expansion of deflationary areas has been observed following urban expansion [Hernández et al., 2007].

3. Methodology

Here we examine the modified regional airflow patterns during four different stages of pre- and post- urban development. Case 1 simulates airflow conditions prior to urbanization. Case 2 simulates flow conditions during the first phase of development in the mid-1960s and early 1970s. During this period the majority of construction took place at Maspalomas and initial human perturbation of the airflow occurred. Case 3 represents the second phase of urbanization where the edges of the terrace were urbanized during the late 1970s and early 1980s. Case 4 represents the last phase of urbanization during the late 1980s and early 1990s. The most recent buildings were added to the southern extent of the terrace surface which extends furthest into the central section of the dune field. Aerial photographs for each stage of urbanization (i.e. Cases 1-4) enable analysis of dunefield response at each time interval. LiDAR surveys from 2006-2011 illustrate characteristic topographic change in the dunefield following the last phase of urbanization.

3.1. Dunefield Geomorphology

The geomorphology of the Maspalomas dunefield was examined using historical aerial photographs from the same time series as the model simulations (i.e. 1961, 1977, 1987, and 2006). These photographs allow for identification of progressive changes in the total land cover area of the dunefield, beach, bare sand, deflation, and vegetation surfaces. Dunefield polygons were identified by manually tracing along the low water mark and around the periphery of dune deposits for each time period. Beach polygons were then extended from the low water mark to the initial dune deposits inland. The remaining data were classified in ArcGIS using the iso-cluster unsupervised classification function. Land cover was classified into three groups (vegetation, deflation or the exposed underlying alluvium layer, and bare sand areas) based on each classes range of RGB values. These geomorphic classes were then manually cleaned or amended by overlaying the data on the original photograph to determine the accuracy of the classification. Vegetation and deflation areas were defined during each time interval and all other areas within the dunefield (i.e. representing sand sheets, stoss slopes, slip faces, etc.) were defined as active sand surfaces that are subject to transport.

Topographic changes at the dunefield were monitored through successive aerial LiDAR surveys from 2006, 2008, and 2011. This allows for the quantification of the topographic and volumetric changes occurring at the study site following the post-urbanization phase. The 2011 dataset was unfiltered and all data above the sand surface (i.e. representing vegetation) was removed and considered null within the measurements. Patches of vegetation were identified in the 2011 survey by running the neighbourhood block statistics function in ArcGIS to determine the standard deviation of the elevation values within a 3 x 3 moving window across the DEM surface. Abrupt spikes, representing the transition between the topography and vegetated areas, were identified from a user defined threshold as areas exceeding two standard deviations (i.e. >0.47) from the mean (i.e. 0.17). Areas identified as vegetation were then used to mask the 2011 DEM, removing any overestimation of the bare earth surface in subsequent topographic measurements. By differencing the model surface we are able to identify key areas of erosion and deposition. Sediment budgets were then created to determine the net volumetric change of sediment within the dunefield between each survey interval.

3.2. Climatic Variability

Climatic variability at Maspalomas was analysed for the period 1957 to 2011. Daily averages of temperature, precipitation and wind speeds were downloaded from the National Oceanic and Atmospheric Administration (NOAA) National Centers for Environmental Information (NCEL) database. Regional climatic data were recorded at an Agencia Estatal de Meteorologia (AEMET) station at the Las Palmas de Gran Canaria Airport (LPA) located 25 km northeast of the dunefield. Daily precipitation (P) and temperature normals were used to predict the annual potential evapotranspiration (PE) using the Thornthwaite [1948] method at the study site per annum. Daily averages for wind speed were used to determine the frequency of winds exceeding the minimum threshold velocity (i.e. 5.5 ms^{-1} for the average 0.22 mm sediment diameter found within the dunefield; [Bagnold, 1941; Smith et al., 2017]) per year (W). Variability in climate was used to determine the dune mobility function (M; Eq. 1) over time to provide an index of climatic controls on dunefield dynamics [Lancaster, 1988]. M values < 50 are considered stable with inactive dunes, 50-100 only dune crests are active, 100-200 dunes are active with vegetated interdunes and lower slopes, and >200 dunes are fully active [Lancaster, 1988].

$$M = W/(P\!:\!PE) \qquad \text{Eq. 1}$$

3.3. CFD Modelling

Modelling of the regional airflow conditions across the study site was conducted in OpenFOAM, an opensource CFD modelling software. For the simulations conducted in this study the Re-Normalization Group (RNG) $k - \varepsilon$ model was implemented because it has relatively low computational costs and the ability to accurately simulate flow conditions in complex three dimensional dune environments [Smith et al., 2017]. Atmospheric boundary layer (ABL) conditions, specified at the model inlet, are free stream velocity (U; Eq. 1), turbulent kinetic energy (k; Eq. 2), and energy dissipation (ε; Eq. 3) [Richards and Hoxey, 1993]. Here u_* represents the shear velocity, K is von Kármán's constant, z is the height of the reference velocity, z_o is the aerodynamic roughness length, and C_μ is a model constant 0.09. Initial conditions were taken as the mean wind velocity exceeding threshold conditions (i.e. 7.2 ms^{-1}) and taken from highest frequency winds (i.e. ENE) occuring at the site for the period of 2006-2013. These ABL conditions were used as the input for all four historical models, representing varying stages of urbanization for the years 1961, 1977, 1987, and 2006 (Fig. 3a).

$$U = \frac{u_*}{K} ln\left(\frac{z+z_o}{z_o}\right) \quad (1)$$

$$k = \frac{{u_*}^2}{\sqrt{C_\mu}} \quad (2)$$

$$\varepsilon = \frac{{u_*}^3}{K(z_o+z)} \quad (3)$$

Buildings were modelled within Trimble SketchUp to provide realistic 3D building geometries and were overlayed onto the the topographic model surface (Fig. 3a,b). All models utilize a LiDAR DEM from 2006 as the characteristic dune topography. Although the dunes are highly dynamic, this DEM acts as a model control to look at the direct impact of buildings on the regional flow patterns through time without the additional variability due to modified bedform-flow interaction. The dunes were designated constant z_o values of 0.1 m [Smith et al., 2017] while the urbanized area was given z_o values of 0.8 [Troen and Lundtang Petersen, 1989]. Jackson and Hunt's [1975] IBL depth (Eq. 4) was used to estimate the minimum refinement of the mesh surface in order to reduce computational costs in areas of free stream while capturing geomorphically relevant near surface flow conditions. The total number of cells within the model domains were ~2x10^7 and varies slightly depending on the number of buildings added to the model surface (Fig. 3a,b). Surface cell normals are reported at a 1m x 1m resolution; however, cells become increasing refined (i.e. < 1m x 1m) in areas of highly heterogenous surface slope (e.g. slip faces and building edges) in order to maintain an accurate surface gradient. Models were run at a sampling rate of every 0.01 s^{-1} and were terminated after convergence was achieved when the residuals of the fluctuating model components of the 3D flow velocity (u, v, w), k, ε, and surface pressure ρ all fell below 0.001.

$$\frac{l}{L} ln\left(\frac{l}{z_o}\right) = 2K^2 \quad (4)$$

Model results were measured directly from the model surface including airflow direction (θ; Eq. 5), turbulence intensity (TI; Eq. 6), and surface shear stress (τ_W; Eq. 7). Where TKE is the turbulent kinetic energy taken as one half of the standard deviation of the three flow components (i.e. u, v, w), U is the mean velocity, u is the horizontal velocity parallel to the model surface, y is the vertical distance to the model wall, and μ is the molecular dynamic viscosity.

$$\theta = atan2(u, v) \quad (5)$$

$$TI = \frac{\sqrt{\frac{2}{3}TKE}}{U} \quad (6)$$

$$\tau_W = \mu \frac{\partial u}{\partial y}_{(y=0)} \quad (7)$$

τ_W was used to estimate the potential sediment flux across the entirety of the model surface following the techniques developed by [Smith et al., 2017]. Surface shear velocity (u_*; Eq. 8) was input to into Sauerrmann et al.'s [2001] saturated sediment transport equation (q_{sat}; Eq. 9). This sediment transport equation acts as potential sediment transport given the modified flow velocity at the surface and better estimates intermediate transport conditions where $u_* \gg u_{*t}$. This equation has performed well during experiments over barchan dune topography and is determined to be a suitable model for the study site [Sauerrmann et al., 2003]. Here ρ represents the specific weight of air, u_{*t} is the threshold shear velocity [Bagnold, 1941], model constants α and z_1 [White and Mounla, 1991], the average height of saltation z_m [Owen, 1964], and u_{st} the minimum velocity of sand grain saltation [Sauerrmann et al., 2001].

$$u_* = \sqrt{\left(\frac{\tau_W}{\rho}\right)} \tag{8}$$

$$q_{sat} = \begin{cases} 2\alpha \frac{\rho}{g}(u_*^2 - u_{*t}^2)\left(u_* \frac{2}{K}\sqrt{\frac{z_1}{z_m} + \left(1 - \frac{z_1}{z_m}\right)\frac{u_{*t}^2}{u_*^2}} - \frac{2u_{*t}}{K} + u_{st}\right) & for\, u_* \geq u_{*t}, \\ 0 & else. \end{cases} \tag{9}$$

Potential sediment transport was corrected using Bagnold's (1973) formula (Eq. 10) relative to the localized slope of the surface (G; Eq. 11). Here α_r is the angle of repose (~34°) and θ_s is the local surface slope. For each time series, reported results were normalized to the initial pre-urbanization model (i.e. t and $\theta_{2,3,4}$) using Jackson and Hunt's [1975] fractional perturbation ratio for q' and TI (Eq. 12). θ was normalized to the unperturbed pre-urbanization model and is reported as the percent change of flow direction from -50% to +50% (Eq. 13).

$$q' = Gq_{sat} \tag{10}$$

$$G = \frac{tan\alpha_r}{cos\theta_s(tan\alpha_r + tan\theta_s)} \tag{11}$$

$$\delta_{(q',TI)} = \frac{t_{(2,3,4)} - t_1}{t_1} \tag{12}$$

$$\Delta_\theta = \frac{\theta_{(2,3,4)} - \theta_1}{360} \tag{13}$$

4. Results

4.1. Land Cover and Topographic Change

The physical extent of the Maspalomas dunefield has been reduced by 17% between 1961 and 2006 (Fig. 4; Table 1). Agricultural encroachment of the dunefield was already occurring prior to 1961; however, the majority of the reduction is due to large scale urban development during the mid-1960s (Fig 4a,b; Table 1). During subsequent construction phases between the 1970s and 1990s the entire southern terrace was urbanized, cutting off the sediment supply to the northwest section of the dunefield (Fig. 4c,d). During this 50 year period three distinct morphological trends are evident in the boundaries of the dunefield: a) a retrograding coastline at Playa de Maspalomas; b) episodic pro- and retro- grading coastline at Cape La Bajeta; and c) stability of the coastline at Playa del Inglés (Fig. 4).

Within the dunefield, large scale land cover changes have been observed at the decadal scale. Bare sand surfaces were reduced by 34% between 1961 and 2006 (Fig 4; Table 1) concomitant with increases of 310% and 145%, respectively in the surface coverage of vegetated and deflation areas. In the active dune area the interdune spacing has increased, evident in continual expansion of deflation areas between dune deposits, particularly adjacent to the source area at Playa del Inglés. Beach area has nearly doubled during the study time period. This is largely attributed to the increased width of Playa del Inglés. The intermittent foredune in the NE section has been stabilized by vegetation over the past twenty years [Hernández Calvento, 2006]; however, in the E/SE extent the development of incipient barchan dunes and barchanoid dune ridges is occurring at increasingly further distances downwind of the sediment source area (Fig. 4).

Topographic changes, measured from repeat aerial LiDAR surveys, indicate a net sediment loss from the Maspalomas dunefield from 2006 to 2011 (Fig. 5a,b). Between 2006 and 2008 234,676 m^3 was lost, primarily from the active section of the dunefield (Fig 5a). Across the northwest section the surface has become highly stabilized and shows only small topographic changes. Similar net sediment loss occurred between 2008 and 2011 when 315,171 m^3 was removed from the dunefield (Fig. 5b). At Playa de Maspalomas the retrograding coastline is encroaching on the dunes in the southwest section of the dunefield with a retreat of up to ~106 m between 1961 and 2006. Migrating dunes show a general trend of reduction in crest height through time. In total the system displays a high level of sediment deficit. At the current rate of net erosion (~110,000 m^3 per year), the 14.1 x 10^6 m^3 of active sediment [Vallejo et al., 2009] could be depleted within ~128 years.

4.2. Climatic Controls

Low precipitation, warm temperatures, and high wind energy promote high dune activity at Maspalomas. Mobility index values 1957- 2011 (Fig. 6) show the dunes to be fully active (i.e. $M > 200$) except during 1957 and 1962 (i.e. $100 < M < 200$). Wind speeds are unavailable for 1963-1964 and 1967-1972. Spikes in M show that certain years have increased erosive potential. The largest M occurs in 1961 when the dune field experienced hyper-arid conditions (i.e. $P\!:\!PE < .05$; [UNCCD, 1994]). Other years recording hyper-arid conditions were 1961, 1963, 1975, 1976, and 1977. All other years recorded arid conditions (i.e. 0.05 – 0.20) except for 1971, 1972, 1989, 1991, 1993, and 2005 which recorded semi-arid conditions (i.e. $P\!:\!PE <$ 0.20-0.50). Fluctuations in aridity have the most direct impact on M at Maspalomas. W remains relatively consistent with an average of 62% of days per year exceeding threshold conditions. There is a slight overall decline in M due to the decrease in drought conditions experienced in the 1960s and 1970s; however, M values have remained relatively high with the potential to promote the development of fully active dunes with limited influence of vegetation stabilizing the surface.

4.3. Regional Airflow and Sediment Transport Dynamics

The initial ABL conditions designated at the CFD domain inlet were specified for each model as U= 7.2 ms^{-1}, u_*= 0.67 ms^{-1}, k = 1.52 m^{2}s^2, θ = 72°, ε = 0.07 m^{2}s^3, and ρ = 0 m^{2}s^2. The only variability in model simulations occurs when adding the representative building geometries through time during Case 2 (1977), Case 3 (1987), and Case 4 (2006). This allows direct comparison of the influence of the different stages of urban construction on the magnitude of regional airflow perturbations, relative to the pre-urbanized airflow conditions represented by Case 1 (1961).

4.3.1. Sediment Flux Potential

Prior to urbanization airflow transitions from the open sea and a relatively flat beach face before acceleration occurs over the accumulation zones in the central section of the dunefield. Here, airflow is compressed and accelerates over elevated barchanoid dune ridges and the alluvial terrace surface leading to higher rates of predicted q' (Fig. 7a). Downwind of the terrace and large barchanoid ridges, there is a natural reduction in q' as energy is dissipated following IBL flow over elevated bedforms with increasing surface roughness (Fig. 6a). During case 2 (Fig. 6b), much of the surface to the E and S of the terrace experiences an increase of 0.20 – 0.40 $\delta q'$ as airflow is modified by the building geometries. The largest increase (>0.40) occurs at the dunes on the boundary of the terrace. Reduction in $\delta q'$ is observed downwind with ranges of values of <-0.80 in the immediate boundary between the urban terrace declining to -0.40 - -0.20 at ~500m downwind and >-0.20 at the W/NW extent of the dunefield (Fig. 7b). Detached flow conditions downwind of the urban terrace do not have sufficient length to reach flow recovery within the shadow zone causing a reduction in $\delta q'$ across the entire NW sector of the dunefield.

Case 3 shows similar results as Case 2, however, the magnitude of surface flow velocity perturbations has increased (Fig. 7c). There is an increase of $\delta q'$ between 0.60 – 0.80 of surface velocity around the urban-dunefield margin at the S end of the terrace. Elevated $\delta q'$ predictions continue towards the southwest of the terrace across barchan dune ridges with an increase of 0.20 – 0.40. At Playa de Maspalomas, $\delta q'$ is less magnified with an increase of up to 0.10 – 0.20 except for the uppermost dune crests which still record an increase of $\delta q'$ up to 0.20 – 0.40. The deceleration of flow in the urban shadow zone is further magnified during Case 3, with much of the surface area experiencing a decrease in $\delta q'$ between -0.40 - -0.20 (Fig. 7c). This area of retarded $\delta q'$ extends further downwind ~1km from the edge of the urban terrace. Further changes to $\delta q'$ in Case 4 are only slightly modified in comparison to Case 3. The largest $\delta q'$perturbations are manifest in the acceleration of flow E and S of the terrace. Here the buildings built during the last construction phase are relatively high and create an amplified localized impact on the regional flow patterns. The dunes near this section of the terrace experience an increase in $\delta q'$ of over 0.80 greater than pre-urbanization conditions (Fig. 7d). Overall, the rest of the dunefield displays similar results to cases 2 and 3 with magnified $\delta q'$ across much of the active dune surface and a subsequent reduction of $\delta q'$ across the majority of the NW section of the dunefield. The first two phases of construction (i.e. Case 2 and 3) had the largest impact on $\delta q'$ causing significant modification of dunefield sediment dynamics in response to urbanization (Fig. 7b,c), with only slight additional modifications occurring following the final phase (i.e. Case 4).

4.3.2. Surface flow direction

Prior to urbanization θ is relatively unperturbed with ENE winds veering slightly towards the NE across much of the active dune surface. Directly downwind of the alluvial terrace, short recirculation cells develop as airflow is detached from the elevated terrace surface and recirculated towards the W base of the terrace (Fig 8a). During Case 2, approaching airflow is shifted slightly to more northerly winds across most of the dunefield. The largest $\Delta\theta$ is recorded across the active section of the dunefield, SW of the terrace surface, with flow being deflected ~12° towards more northerly winds compared to unperturbed flow conditions prior to urbanization. Across the urbanized surface, the $\Delta\theta$ across the buildings, inter-building (i.e. streets and parks), and downwind of the terrace are greatly modified (Fig 8b). Recirculation cells with increased lengths (~125 m) begin to develop in response to buildings being added to the W surface of the terrace.

Case 3 displays larger magnitudes of $\Delta\theta$ with winds being shifted up to 12° northerly as airflow approaches the windward side of the terrace and 12° easterly downwind of the terrace (Fig. 8c). Airflow on the windward side of the terrace is being redirected towards the southwest before flow begins to shift towards the west as airflow moves around the terrace. This suggests that airflow is being compressed and redirected before expansion occurs downwind of the terrace as flow conditions begins to normalise. In the immediate lee of the urban terrace, large scale recirculation cells are developed with flow being recirculated up to 162° from the unperturbed surface directions. Case 4 displays similar patterns, however, the magnitude of $\Delta\theta$ is again increased. The dune ridges to the E of the terrace experience northerly flow deflection of ~25° (Fig 8d). As airflow moves around the terrace a ~21° easterly deflection of winds occurs across the western section of the dunefield. The recirculation cells increase in length by >200 m downwind of the prominent buildings added in the last phase of urbanization. Each phase of construction had a significant impact on $\Delta\theta$; however, the intensity of steering increased the most during Cases 3 and 4.

4.3.3 Surface Turbulence Intensity

Case 1 displays a surface with TI values largely between 1.25-1.75, with elevated values occurring in the lee of higher dune crests in the central section of the dune field and downwind of the alluvial terrace (Fig. 9a). Subsequent cases show an increase in δTI values across the urbanized terrace, in the lee of the dune crests, and interdune areas while displaying a drop in δTI across the stoss slopes. This acceleration across the stoss slopes reduces δTI values, where sediment flux is usually controlled by the generation of streamwise stress as airflow accelerates towards the crest. As flow detachment occurs at the crest, highly turbulent flow conditions transfer momentum towards the surface from the overlying wake zone causing increase in TI. This leads to intermittent erosive potential due to turbulent forces that are not accounted for in the q' estimates. Increase in δTI can also potentially lead to increased dune spacing as sediment is being either recycled back towards the lee slope base in response to recirculating vortices or further downwind to the next dune deposit as the IBL begins to normalize beyond the point of reattachment [Walker and Nickling, 2002; Baddock et al., 2007].

Highly turbulent coherent flow structures, in the form of two counter-rotating vortices, are identified across much of the dune topography that experiences recirculating secondary airflow patterns. These correspond with elevated TI and δTI in the lee-side locations, indicated in red (Fig. 9a,b,c,d). The ubiquity of these features across much of the dunefield surface suggests they have a significant influence on dune spacing. Elevated δTI is recorded in many lee slope and interdune surfaces following urbanization, potentially accelerating the erosive potential in low velocity environments. δTI is largely modified following the initial construction phase, represented in Case 2, with subsequent Cases (i.e. 3 and 4) showing only a slight increase in δTI magnitude. The shadow zone also displays elevated δTI values following urbanization (Fig. 9b,c,d). Bare sand deposits, not stabilized by the sheltering effect of vegetation, have the potential to be reworked despite the drop in q'.

This corresponds well with the observed topographic changes showing areas of both low magnitude erosion and deposition. Given the limitations of the influx of new sediment to this region, all topographic changes are assumed to involve redistribution of pre-existing deposits. Progressive construction phases display an increase in δTI magnitude and length downwind of the terrace, displaying the progressively intensified turbulent nature of flow over the urban area.

5. Discussion

Since urbanization of the alluvial terrace at Maspalomas began during the mid-1960s there has been clear dichotomy of geomorphic evolution of the dunefield. In the urban shadow zone, large scale stabilization is manifest in an exponential increase of vegetation that anchors existing dune forms. Redistribution of sediment occurs over the pre-existing bare sand deposits and deflation areas. In contrast, the acceleration zone has seen increased sediment transport due to increased velocity of airflow across the active dune surfaces. Increased $\delta q'$ has led to the overall lowering of the dune crests and increase in deflation areas as the erosive potential exceeds sediment input into the system. Although there has been a reduction of predicted M through time (Fig. 6), it is clear that the controls on dunefield dynamics, defined by Kocurek and Lancaster [1999], have been significantly altered by urban development. The authors proposed an ‘Aeolian System Sediment State’ model that suggests dunefields are controlled by three over-arching variables: sediment supply, susceptibility of sediment to be transported, and the competence of the local wind regime. In this context, our study site displays a sediment supply that has remained relatively constant with the source area at Playa del Ingles experiencing equilibrium over the last 50 years; however, the urban shadow zone has been directly cut off from new sediment inputs by urban development starving the northwest sector of new sediment influx. The susceptibility of sediment to transport has decreased due to both the increase in vegetation in the urban shadow zone and deflation areas in the acceleration zone. This is directly linked to the reduction of bare sand surfaces available for sediment transport and is characteristic of a dune system that is in decline. Lastly, there has been a decrease of the competent wind regime downwind of the urban area and an increase in airflow competence in the active section of the dunefield promoting both retarded and elevated rates of erosion in both respective regions of the dunefield.

The dynamism of dunefield evolution has often been linked to fluctuations in climatic variables including W, P, and PE [Lancaster, 1987; Muhs and Maat, 1993; Wiggs et al., 1995; Stetler and Gaylord, 1996; Wolfe, 1996; Bullard et al., 1997; Lancaster, 1997; Lancaster and Helm, 2000; Muhs et al., 2003; Hugenholtz and Wolfe, 2005; Thomas et al., 2005]. At the dunefield scale, it is unusual to find accelerated or re-activated transport and stabilization during the same climatic conditions. Simultaneous dunefield stabilization and increased mobilization have been identified in the Negev-Sinai desert and the coastal sand dunes in Ceará State in Northeast Brazil [Yizhaq et al., 2007; Tsoar et al., 2009]. In the Ceará State dunefield, this was attributed to the seasonality of strong wind conditions that can lead to the degradation of vegetation in spatially limited areas causing the reactivation of the underlying sediment. In the Negev-Sinai desert, variability in dunefield mobility is due to human land use differences on the Egyptian (grazing and gathering) and Israeli (inactive) sides [Meir and Tsoar, 1996; Yizhaq et al., 2007]. While these studies provide evidence that both climatic and human impacts have an effect on the mobility of dunefields, they are still relatively limited because they do not account for the perturbations of IBL flow conditions as a result of dune topography or other regional controls [Bullard et al., 1997]. Our work shows that urbanization, adjacent to dunefields, can have a direct impact on IBL airflow and can significantly alter regional airflow dynamics and geomorphic evolution at the dune and dunefield scale.

Hernández-Calvento et al. [2014] conducted the first model to analyse the impact of urbanization on the regional airflow perturbations across a dunefield. Here we build upon this original study by providing a coupled meso-scale CFD model using detailed building geometries and actual dune topography. The perturbations of regional airflow from urbanization development and associated impacts on a natural dunefield systems has provided highly detailed information on actual modifications of sediment flux potential, directionality, and TI. These modified flow patterns have had a deterministic impact on the geomorphology of the dune system and has led to both the simultaneous stabilization and acceleration of erosion within the dunefield. This has fundamentally transformed the system at the decadal scale to adjacent areas of highly stabilized and increasingly activated dune dynamics, overriding limited fluctuations in climatic variability.

5.1. Land Cover and Topographic Change

Despite the negative sediment budget of the dunefield and marine deposits [MMA, 2007; Bouzas et al., 2013], there has been an equilibrium of the dune system source area deposits at Playa del Inglés over the past 50 years [Fontan et al.,2012; Quevedo Medina and Hernández-Calvento, 2014]. This suggests a relatively consistent supply of sediment at the decadal scale. At this same temporal scale, urbanization on the alluvial terrace and NW edge of the dunefield has directly reduced the areal extent of the dunefield (Fig 4). Further reduction of the dunefield area is also evident in the retro-gradation of the Playa de Maspalomas coastline with retreat of up to ~105 m between 1961 and 2006 in response to SW storm events [Bouzas et al., 2013]. These trends have accounted for a loss of 17% of total area during this time period (Table 1). Although there is a stable input of sediment into the system, the coupled natural and anthropogenic dynamics of the environment has led to the overall decrease in dunefield area, increase in vegetation and deflationary areas, decreased bare sand surfaces, increased distance between dune deposits and the source area, and overall lowering of the dune topography.

The increase in vegetation and subsequent stabilization of the shadow zone can be attributed to two major factors that have disrupted the natural system. The sediment corridor has been shifted to flow around the south of the terrace and bypassing the urban shadow zone. This, coupled with a decrease in competent airflow and sediment flux potential, has led to widespread colonization of plant species [Hernández-Cordero et al., 2015a,b]. Previous studies have found that dune vegetation causes an exponential decrease in sediment flux [Wiggs *et al*., 1996b; Lancaster and Baas, 1998; Lancaster, 2000]. Lancaster and Baas [1998] stated that the sediment flux is reduced by 90% of the bare sand surface values when vegetation covers just 12% of the surface area. Wiggs et al. [1996b] proposed a threshold vegetation cover of 14% at the dune scale, where the onset of stabilization occurs. Much of the remaining dunes have become vegetated within the shadow zone. These are interspersed with intermittent areas of bare sand and deflation surfaces (Fig. 4). Between 1961 and 2006, vegetation within the shadow zone increased from 6% to 23% of the total area suggesting the development of a new system equilibrium, identified by large scale stabilization in response to urbanization.

Deflation areas have also increased through time, particularly within the acceleration zone (Fig. 4). The most significant increase is at the E edge of the dunefield [Hernández-Calvento et al., 2014]. Hernández et al. [2007] found the accumulation ridge (i.e. coalescence of incipient barchans into larger barchanoid ridges) has occurred at an increasing distance from the sediment source area at Playa del Inglés. This has led to a significant rise in deflation surfaces in this region as small incipient barchan dunes migrate rapidly across the underlying alluvium layer at up to 35 m yr^{-1} [Jackson et al., 2013b]. This in part, can be attributed to other anthropogenic pressures caused by trampling of the near shore vegetation leading to fragmentation of the foredune and rapid sediment migration further inland [Hernández-Cordero et al., 2012; Hernández-Calvento et al., 2014]. Near the terminus section, adjacent to Playa de Maspalomas, an increase in deflationary surfaces has also been observed on the border between the urban shadow and acceleration zones. These areas receive reduced sediment inputs due to the deflection of the sediment and airflow across the dunefield. The rise in deflation areas throughout the dunefield has shifted the system into an availability-limited state [Kocurek and Lancaster, 1999], and suggests that changes in the wind energy have resulted in accelerated erosion as dune migration rates exceed sediment input into the system.

Topographic changes, between 2006 and 2011 (Fig. 5), gives an insight into any sediment deficit occurring at the Maspalomas dunefield. During this time, average climatic conditions showed slightly elevated M values in 2009 due to below-average P and above average PE and W (Fig. 6). Despite this spike in predicted dune activity for 2009, the lowering of the dune topography and the rates of volumetric changes occurring in the system remain relatively constant with an average of ~110,000 m³ of net erosion of sediment leaving the system per year at the sub-decadal scale. Limited sample size only provides a brief understanding of the sediment budget of the Maspalomas dunefield; however, it indicates its sediment-limited nature. Given the current available sediment volume of 14.1 x 10^6 m³ and the rates of sediment loss, the remaining sediment could be removed within ~128 years. Most of the erosion is concentrated in the acceleration zone, where bare sand surfaces predominate and are positioned away from the stabilizing effect of vegetation. Here, elevated sediment flux potential is predicted due to the magnification of regional airflow in response to the urban geometry. In contrast to the positive feedback identified in the vegetated urban shadow zone, the impact of urbanization appears to have a negative feedback upon the active dune surfaces leading to both the acceleration of deflation and erosion across much of the dune surfaces due to modified regional flow dynamics.

5.2. Regional Airflow and Sediment Transport Dynamics

Sediment transport prior to urbanization showed increased flux magnitude over the elevated dune ridges reaching a maximum at the dune crests (Fig. 7a). This is consistent with streamline compression and acceleration of airflow up the stoss slopes of the dunes, leading to increased streamwise shear stress at the surface [Frank and Kocurek, 1996a; Wiggs et al., 1996a; Walker and Nickling, 2002]. Perturbations associated with the first phase of urbanization (Case 2) caused increased sediment flux magnitude across the acceleration zone and decreased flux in the urban shadow zone in the NW sector of the dunefield (Fig. 7b). Subsequent perturbations, during Cases 3 and 4, show similar spatial patterns (Fig. 7c,d), however, the magnitude increases through time. Following urbanization, flux potential increased by > 0.80 across the dune crests on the southern tip of the terrace and decreased by a similar amount in the immediate lee of the buildings. These modified flux patterns has had a significant impact on the dune dynamics and in- stability identified in the geomorphic analysis at each time step.

The shadow zone has experienced large scale stability due to the reduction of velocity in the lee of the urban terrace. Recovery of airflow, where surface shear stress normalizes to upwind values, has been estimated to between 18-30h (where h is the obstacle height) [Walker and Nickling, 2003]. Separated flow conditions, downwind of the buildings on the western edge of the terrace, however, do not recover to upwind flow conditions due to the limited lateral extent of the dunefield. Thus, modified flux dynamics downwind of the dunefield never fully re-develop to unperturbed shear stress values allowing for the widespread stabilization of the urban shadow zone. In contrast, the acceleration zone experiences magnified flux potentials as airflow is compressed and accelerated around the building geometries. This leads directly to intensified surface shear stress over the majority of the dune surfaces and explains the accelerated erosion observed at the site through time. As the dune surfaces are lowered, the recovery of flow occurs at shorter lengths across isolated interdune locations in the eastern section of the dunefield. This has led to the accelerated dune migration, increase in deflation areas, and an increase in distance from the source area to the main accumulation ridge in the central section of the dunefield [Hernández et al., 2007; Jackson et al., 2013b]. In the central and southwestern sections, sediment flux is also intensified and these locations have displayed the highest rates of net topographic lowering (Fig. 5a,b).

Significant $\delta\theta$ has also been observed at Maspalomas where largely homogeneous flow directions are observed during the pre-urbanization phase to highly deflected flow in subsequent urbanization phases. The initial perturbations caused by the first phase of urbanization, deflected flow northerly upwind of the terrace moving sediment towards the S before flow moving around the terrace redirects easterly moving sediment towards the W in downwind locations (Fig. 8b). Following each phase of urbanization and resulting flow perturbations (i.e. Cases 3 and 4) we see, relative to pre-urbanized flow directions, a magnification of flow deflection of up to 25° upwind of the terrace, 21° downwind of the terrace, and 172° in the urban induced recirculation cell relative to pre-urbanized flow directions. These results correspond well with those presented by Hernández-Calvento et al. [2014] who found a 15° – 20° deflection of flow upwind of the terrace before flow shifted towards the S in downwind locations. The geomorphic significance of these perturbations is the modification of primary (i.e. stoss side flow) and secondary (i.e. lee side flow) at the dune length scale and the overall truncation of the sediment pathway through the system at the dunefield scale.

As wind moves across the individual dune topography, the incident angle of airflow has significant impact on the secondary airflow dynamics that occur in the lee. Sweet and Kocurek [1990] found that incident angles of 90° ± 15° produced the development of 15° – 75° roller vortices, and deflected flow by 10° - 70°. These in turn have significant impact on sediment transport dynamics with recirculating turbulent vortices recycling sediment back towards the lee slope and maintaining characteristic dune-form geometries [Tsoar and Yaalon, 1983; Tsoar et al., 1985; Sweet and Kocurek, 1990; Frank and Kocurek, 1996b; Walker, 2000; Smith et al., 2017]. For example, the deflection of lee-side flow direction increases through time due to the upwind flow being forced to a more northerly angle with $\delta\theta$ of up to 25° during Case 4 (Fig. 8d), modifying the approach angle on the stoss and thus potentially modifying the secondary airflow dynamics (e.g. deflected flow vs. recirculating vortices) [Lynch et al., 2010]. At the dunefield scale, surface flow direction and subsequent sediment inputs into the system from Playa del Inglés are therefore being forced towards the south accumulating mainly in the central section of the dunefield. Here, velocity acceleration and deflection towards the S leads to a shortened sediment corridor in which the migration of dunes can take place. This potentially leads to the reduction of residence time of sediment being fed into the dunefield, further amplifying the sediment deficit recorded at Maspalomas.

Following urbanization there has been an increase of δTI, primarily on the lee slopes of elevated dune crests in the central section of the dunefield and in the interdune areas where secondary airflow patterns are observed. This increase in δTI can lead to intermittent sediment transport due to the momentum transfer of the overlying turbulent wake zone to the surface near the point of reattachment [Walker and Nickling, 2002; Baddock et al., 2007]. Our results also show elevated values of δTI on the lee slopes providing elevated erosive potential due to destabilizing concave curvature in mobilizing sediment under low threshold values [Wiggs et al., 1996a; Smith et al., 2017]. Coherent flow structures are also apparent and are identified by an elevated δTI signature (Fig. 9a,b,c,d). Smith et al. [2017] found evidence of coherent counter-rotating vortices that develop over barchan dunes in highly turbulent secondary airflow conditions in the lee. These counter-rotating vortices have also been modelled in terrestrial [Feng and Ning, 2010] and subaqueous [Omidyeganeh et al., 2013] dunes. The prevalence of these structures in the lee of dune crests (Fig. 10a) displays a commonality in turbulent flow that likely has a deterministic impact on dune morphology and dynamics. Smith et al. [2017] suggested that these flow structures could work to maintain the characteristic crescentic shape of barchan dunes by redirecting sediment back to the base of the lee slope centreline and laterally away towards the inner barchan arms across the lee slope.

Across the urban area and the downwind urban shadow zone, highly turbulent airflow conditions develop (Figs. 9b,c,d; 10b). Increased surface roughness due to urbanization caused an increase in δTI compared to the relatively stable flow conditions observed during pre-urbanization (Fig. 9a). Well-developed recirculation cells form in the immediate lee of the terrace with a range of structures including roller and counter-rotating vortices (Fig. 10a). Increased TI can lead to the redistribution of pre-existing sediment deposits in the urban shadow zone evidenced by low magnitude erosion and deposition between 2006 and 2011 (Fig. 5a,b), despite increased vegetation and the reduced surface velocity. Although increased turbulence may rework existing sediment, fully turbulent flow conditions in the urban shadow zone coupled with limited recovery distance and lack of dune deposits extending into the boundary layer impedes significant sediment transport in this region as flow has insufficient length to recover [Walker and Nickling, 2002].

6. Conclusion

This study provides evidence of regional airflow perturbations and geomorphic implications of anthropogenic structures on IBL flow and dune dynamics. The main conclusions are:

1. Episodic variability in climatic conditions cannot account for the observed changes in the Maspalomas dunefield. Simultaneous stabilization seen from increases in vegetation and accelerated activity seen by sediment deficit is due to the anthropogenic pressure caused by the intrusion of the urban geometry into the IBL.
2. Human-modified regional airflow and sediment transport patterns have led directly to a dichotomy in dunefield evolution (i.e. both increased stabilization and acceleration of erosion) at the decadal scale. This can be attributed to the increasingly magnified perturbations of regional airflow by urbanization during different phases of construction causing two distinct geomorphic zones (i.e. the urban shadow zone and acceleration zone).
3. The urban shadow zone, located downwind of the urban terrace, is largely a stabilized dune system with q' progressively declining due to the reduction in near surface velocity. The sediment input pathway from the source area to the NW sector has largely been cut off with $\delta\theta$ redirecting sediment towards the central section of the dunefield. Also, construction of an impenetrable urban surface further starves this area of sediment, allowing for further colonization of plant species due to the reduction dune migration rates.
4. The acceleration zone, where the active dunes are migrating, has experienced large scale modifications in $\delta\theta$, forcing sediment towards the south and $\delta q'$ thus increasing the erosive potential across much of the active surface. This has led to a progressive deficit in sediment by accelerating erosion and shortening the sediment pathway

through the system, effectively reducing the residence time sediment moves from the source to the terminus.

5. δTI was intensified following urbanization, primarily on the lee slopes and interdune areas. This helps promote intermittent erosion and increased dune spacing, leading to the potential for further acceleration of dune migration and erosion within the system. Coherent turbulent flow structures were identified in the lee of elevated dune crests and downwind of the urban terrace where the development of counter-rotating vortices formed. The ubiquity of these features suggests that they have an important role in both characteristic individual barchan dune form and indeed larger dunefield dynamics.

Acknowledgements

The authors would like to thank the GFyMA Group (IOCAG-ULPGC) for providing resources and logistical support. Expert guidance on CFD modelling and OpenFOAM were provided by Meiring Beyers (Klimaat Consulting & Innovation Inc.). Research funding were provided by the University of Ulster Vice Chancellor's Research Scholarship (VCRS). This work is a contribution towards project CSO2013-43256-R funded by the R&D+I (innovation) Spanish National Programme and a contribution to the UK Natural Environment Research Council grant NE/F019483/1. Any additional information can be requested from the corresponding author at smith-a22@email.ulster.ac.uk.

References

Alcántara-Carrió, J., Fontán, A. 2009. Factors Controlling the Morphodynamics and Geomorphologic Evolution of a Cuspate Foreland in a Volcanic Intraplate Islands (Maspalomas, Canary Islands). Journal of Coastal Research 56: 683-687.

Alonso I., Hernández Calvento L., Alcántara-Carrió J., Cabrera-Vega L.L., Yanes A. 2011. Los grandes campos de dunas actuales de Canarias. In: Sanjaume, E. y Gracia, F.J (Eds.): *Las dunas en España*. Madrid: Sociedad Española de Geomorfología: 467-495.

Baddock, M.C., Livingstone, I., Wiggs, G.F.S. 2007. The geomorphological significance of airflow patterns in transverse dune interdunes. Geomorphology (87): 322-336.

Bagnold, R.A. 1941. The physics of wind-blown sand and desert dunes. Methuen, London, 265 (10).

Bagnold, R.A. 1973. The nature of saltation and of 'bed-load' transport in water. In Proceedings of the Royal Society of London A: Mathematical, Physical and Engineering Sciences. Vol. 332. no. 1591: 473-504.

Bai, J.J., Park, S.B. 2009. Urban Flow and Dispersion Simulation Using a CFD Model Coupled to a Mesoscale Model. Journal of Applied Meteorology and Climatology (8): 1667-1681.

Bauer, B.O., Walker, I.J., Baas, A.C.W., Jackson, Derek, McKenna-Neuman, C., Wiggs, G.F.S. and Hesp, P.A. (2013) Critical Reflections on the Coherent Flow Structures Paradigm in Aeolian Geomorphology. In: Venditti, J.G., Best, J.L., Church, M., Hardy, R.J. (Eds.), Coherent Flow Structures at Earth's Surface, Wiley, pp. 111-134. ISBN: 978-1-119-96277-9.

Blocken, B., Janssen, W.D., van Hoof, T. 2012. CFD simulation for pedestrian wind comfort and wind safety in urban areas: General decision framework and case study for the Eindhoven University campus. Environmental Modelling & Software (30): 15-34.

Bouzas, A.F., Alcántara-Carrió, J., Montes, I.M., Ojeda, A.B., Albarracín, S., de Rada, J.R.D., Salgado, J.R. 2013. Distribution and thickness of sedimentary facies in the coastal dune, beach, and nearshore sedimentary system at Maspalomas, Canary Islands. Geo-Marine Letters (33;2-3): 117-127.

Bullard, J.E., Thomas, D.S.G., Livingstone, I., Wiggs, G.F.S. 1997. Dunefield activity and interactions with climatic variability in the southwest Kalahari Desert. Earth Surface Processes and Landforms (22): 164-174.

Cabrera-Vega, L.L., Cruz-Aver, N., Hernández-Calvento, L., Hernández-Cordero, A.I., Fernández-Cabrera, E. 2013. Morphological changes in dunes as an indicator of anthropogenic interferences in arid dune fields. Journal of Coastal Research. (65): 1271-1276.

Fadl, M.S., Karadelis, J. 2013 CFD Simulations for Wind Comfort and Safety in Urban Area: A Case Study of Coventry University Central Campus. Internation Journal of Architecture, Engineering, and Construction (2): 131-143.

Feng, S., Ning, H. 2010. Computational simulations of blown sand fluxes over the surfaces of complex microtopology. Environmental Modelling & Software (25): 362-367.

Fontán, A., Alcántara-Carrió, J., Correa, I.D. 2012. Combined beach-inner shelf erosion in short and medium term (Maspalomas, Canary Islands). Geologica Acta (10; 4): 411-426.

Frank, A. and Kocurek, G. 1996 (a). Airflow up the stoss slope of sand dunes: limitations of current understanding. Geomorphology (17): 47–54.

Frank, A., Kocurek, G. 1996 (b). Toward a model for airflow on the lee side of Aeolian dunes. Sedimentology (43): 451-458.

Gundlach, E.R., Siah, S.J. 1987. Cause and Elimination of the Deflation Zones Along the Atlantic City (New Jersey) Shoreline. Coastal Zone'87: 1357-69.

Hanna, S.R., Brown, M.J., Camelli, F.E., Chan, S.T., Coirier, W.J., Hansen, O.R., Huber, A.H., Kim, S., Reynolds, R.M. 2006. Detailed Simultations of Atmospheric Flow and Dispersion in Downtown Manhattan An Application of Five Computational Fluid Dynamics Models. Bulletin of the American Meteorological Society (December 2006): 1713-1726.

Hernández Calvento, L. 2006. Diagnóstico sobre la Evolución del Sistema de Dunas de Maspalomas (1960-2000). Ed. Cabildo de Gran Canaria, Las Palmas de Gran Canaria.

Hernández, L., Alonso, I., Sánchez-Pérez, I., Alcántara-Carrió, J., Montesdeoca, I. 2007. Shortage of sediments in the Maspalomas dune field (Gran Canaria, Canary Islands) deduced from the analysis of aerial photographs, foraminiferal content, and sediment transport trends. Journal of Coastal Research (23; 4): 993-999.

Hernández-Calvento, L., Jackson, D.W.T., Medina, R., Hernández-Cordero, A.I., Cruz, N., Requejo, S. 2014. Downwind effects on an arid dunefield from an evolving urbanised area. Aeolian Research (15): 301-309.

Hernández-Cordero, A.I., Pérez-Chacón, E., Hernández-Calvento, L., 2012. La investigación como soporte de la gestión: el ejemplo de la duna costera (foredune) de Maspalomas (Gran Canaria, Islas Canrias). In: Rodríguez-Perea, A., Pons, G.X., ROig-Munar, F.X., Martín-Prieto, J.A., Mir-Gual, M., Cabrera, J.A. (Eds.). La gestión integrada de playas y dunas: experiencias en Latinoamérica y Europa. Mnografies de la Societat d'História Natural de les Balears 19. Societat d'História Natural de las Balears, PM, Spain: 289-306.

Hernández-Cordero, A.I., Pérez-Chacón, E., Hernández-Calvento, L. 2015. Vegetation disturbance on the coast, and aeolian geomorphic processes and landforms in a transgressive arid coastal dune system. Physical Geography (30; 1): 60-83.

Hernández-Cordero, A.I., Hernández-Calvento, L., Espino, E.P.C. 2015 (b). Relationship between vegetation and dune mobility in an arid transgressive coastal system, Maspalomas, Canary Islands. Geomorphology (238): 160-176.

Hugenholtz, C.H., Wolfe, S.A. 2005. Recent stabilization of active sand dunes on the Canadian prairies and relation to recent climate variations. Geomorphology (68; 1-2): 131-147.

Jackson, P.S., Hunt, J.C.R. 1975. Turbulent wind flow over a low hill. Quarterly Journal of the Royal Meteorological Society 101(430): 929-955.

Jackson, D.W.T., Beyers, M., Delgado-Fernandez, I., Baas, A.C.W., Cooper, J.A.G. and Lynch, K. 2013a. Airflow reversal and alternating corkscrew vortices in foredune wake zones during perpendicular and oblique offshore winds. Geomorphology (187): 86-93.

Jackson, D.W.T., Cruz-Avero, N., Smyth, T., Hernández-Calvento, L. 2013b. 3D airflow modelling and dune migration patterns in an arid coastal dune field. Journal of Coastal Research, Special Issue (65): 1301-1306.

Jackson, N.L., Nordstrom, K.F. 2011. Aeolian sediment transport and landforms in managed coastal systems: A review. Aeolian Research (38): 2011.

Kim, J.J., Fernando, H.J.S. 2003. A CFD Model for Simulating Urban Flow and Dispersion. Journal of Applied Meteorology (42): 1636-1648.

Kocurek, G., Lancaster, N. 1999. Aeolian system sediment state: theory and Mojave Desert Kelso dune field example. Sedimentology (46): 505-515.

Lancaster, N. 1988. Development of linear dunes in southwestern Kalahari, Southern Africa. Journal of Arid Environments (14): 233-244.

Lancaster, N. 1997. Response of eolian geomorphic systems to minor climate change: examples from the southern Californian deserts. Geomorphology (19): 333-347.

Lancaster, N., Baas, A. 1998. Influence of vegetation cover on sand transport by wind: Field studies at Owens Lake, California. Earth Surface Processes and Landforms (23): 69-82.

Lancaster, N., Helm, P. 2000. A Test of Climatic index on dune mobility using measurements from the southwestern United States. Earth Surface Processes and Landforms (25): 197-207.

Lynch, K., Jackson, D.W., Cooper, J.A.G. 2010. Coastal foredune topography as a control on secondary airflow regimes under offshore winds. Earth Surface Processes and Landforms (35.3): 344-353.

Lynch, K., Delgado-Fernandez, I., Jackson, Derek, Cooper, Andrew, Baas, A.C.W and Beyers, J.H.M. 2013. Alongshore variation of aeolian sediment transport on a beach under offshore winds. Aeolian Research (8): 11-18.

Lynch, K., Jackson, D.W.T. and Cooper, J.A.G. 2016. The fetch effect on aeolian sediment transport on a sandy beach: a case study from Magilligan strand, Northern Ireland. Earth Surface Processes and Landforms (41): 1129-1135.

Meir, A., Tsoar, H. 1996. International Borders and Range Ecology: The Case of Bedouin Transborder Grazing. Human Ecology (24): 39-64.

MMA, 2007. *Estudio integral de la playa y dunas de Maspalomas (Gran Canaria).* Technical report. Ministerio de Medio Ambiente, Gobierno de España.

Murakami, S., Ooka, R., Mochida, A., Yoshida, S., Kim, S. 1999. CFD analysis of wind climate from human scale to urban scale. Journal of Wind Engineering and Industrial Aerodynamics (81): 57-81.

Muhs, D.R., Maat, P.B. 1993. The potential response of eolian sands to greenhouse warming and precipitation reduction on the Great Plains of the U.S.A. Journal of Arid Environments (25): 351-361.

Muhs, D.R., Reynolds, R.L., Been, J., Skipp, G. 2003. Eolian sand transport pathways in the southwestern United States: importance of the Colorado River and local sources. Quaternary International (104): 3-18.

Nordstrom, K.F., McCluskey, J.M. 1984. Considerations for control of house construction in coastal dunes. Coastal Management (12): 385-402.

Nordstrom, K.F. 1994. Beaches and dunes of human-altered coasts. Progress in Physical Geography (18): 497-516.

Nordstrom, K.F., Jackson, N.L. 1998. Aeolian transport of sediment on a beach during and after rainfall, Wildwood, NJ, USA. Geomorphology (22): 151-157.

Omidyeganeh, M., Piomelli, U., Christensen, K.T., Best, J.L. 2013. Large Eddy Simulation of flow over barchans dunes. Marine and River Dune Dynamics (15 & 16): 191-198.

Owen, P. R. 1964. Saltation of uniform grains in air. Journal of Fluid Mechanics 20(2): 225-242.

Pullen, J., Boris, J.P., Young, T., Patnaik, G., Iselin, J. 2005. A comparison of contaminent plume statistics from a Gaussian puff and urban CFD model for two large cities. Atmospheric Environment (39): 1049-1068.

Quevedo Medina, U., Hernández Calvento, L. 2014. Evolución reciente de la línea de costa de un sistema playa-dunas deficitario. Maspalomas, Gran Canaria. In: Ramón Morte, A. et cols. (Eds.): Tecnologías de la información geográfica para nuevas formas de ver el territorio. Alicante: Universidad de Alicante, España: 163-171.

Richards, P. J., Hoxey, R.P. 1993. Appropriate boundary conditions for computational wind engineering models using the k-ε turbulence model. Journal of Wind Engineering and Industrial Aerodynamics (46 & 47): 145-153.

Richards, P. J., Hoxey, R. P. 2012. Pressures on a cubic building – Part 1: Full-scale results. Journal of Wind Engineering and Industrial Aerodynamics (102): 72-86.

Sabatino, S.D., Buccolieri, R., Pulvierenti, B., and Britter, R. 2007. Simulations of pollutant dispersion within idealised urban-type geometries with CFD and integral models. Atmospheric Environment (41): 8316-8329.

Sauermann, G., Kroy, K., Herrmann, H.J. 2001. Continuum saltation model for sand dunes. Physical Review E 64(3): 031305.

Sauermann, G., Andrade Jr., J.S., Maia, L.P., Costa, U.M.S., Araújo, A.D., Herrmann, H.J. 2003. Wind velocity and sand transport on a barchan dune. Geomorphology (54): 245-255.

Smith, A.B., Jackson, D.W.T, Cooper, J.A.G. 2017. Three-dimensional airflow and sediment transport patterns over barchan dunes. Geomorphology (278): 28-42.

Smyth, T.A.G. 2016. A review of Computational Fluid Dynamics (CFD) airflow modelling over aeolian landforms. Aeolian Research (22): 153-164.

Stetler, L.D., Gaylord, D.R. 1996. Evaluating eolian-climatic interactions using a regional climate model from Hanform, Washington (USA). Geomorphology (17): 99-113.

Sweet, M.L., Kocurek, G. 1990. An empirical model of aeolian dune lee-face airflow. Sedimentology (37): 1023-1038.

Thomas, D.S.G., Knight, M., Wiggs, G.F.S. 2005. Remobilization of southern African desert dune systems by twenty-first century global warming. Nature Letters (435): 1218-1221.

Thornthwaite, C.W. 1948. An Approach toward a Rational Classification of Climate. Geographical Review (38): 55-94.

Troen, I, Petersen, E.L. 1989. European wind atlas. Roskilde: Riso National Laboratory (1989): 1.

Tsoar, H., Yaalon, D.H. 1983. Deflection of sand movement on a sinuous longitudinal (seif) dune: use of fluorescent dye as tracer. Sedimentary Geology (36): 25-39.

Tsoar, H., Rasmussen, K.R., Sorensen, M., Willets, B.B. 1985. Laboratory studies of flow over dunes. Proceedings of international workshop on the physics of blown sand. Department of Theoretical Statistics, Institute of Mathematics, University of Aarhus. 327-50.

Tsoar, H., Levin, N., Porat, N., Maia, L.P., Herrmann, H.J., Tatumi, S.H., Claudino-Sales, V. 2009. The effect of climate change on the mobility and stability of coastal and sand dunes in Ceará State (NE Brazil). Quaternary Research (71): 217-226.

UNCCD. United Nations Convention to Combat Desertification, Intergovernmental Negotiating Committee For a Convention to Combat Desertification, Elaboration of an International Convention to Combat Desertification in Countries Experiencing Serious Drought and/or Desertification, Particularly in Africa. U.N. Doc. A/AC.241/27. 33 I.L.M. 1328 New York: United Nations; 1994.

Vallejo I., Hernández Calvento L., Ojeda J., Máyer P., Gómez Molina A. 2009. Caracterización morfométrica y balance sedimentario en el sistema de dunas de Maspalomas (Gran Canaria) a partir de datos LiDAR. Revista de la Sociedad Geológica de España 22 (1-2): 57-65.

Walker, I.J. 2000. Secondary airflow and sediment transport in the lee of transverse dunes, Ph. D. Thesis, Department of Geography, University of Guelph. 1-256.

Walker, I.J., Nickling, W.G. 2002. Dynamics of secondary airflow and sediment transport over and in the lee of transverse dunes. Progress in Physical Geography (26): 47-75.

Walker I.J., Nickling, W.G. 2003. Simulation and measurement of surface shear stress over isolated and closely spaced transverse dunes in a wind tunnel. Earth Surface Processes and Landforms (28): 1111-1124.

White, B.R., Mounla, H. 1991. An experimental study of Froude number effect on wind-tunnel saltation. Aeolian Grain Transport (1): 145-157.

Wiggs, G.F.S., Thomas, D.S.G., Bullard, J.E. 1995. Dune mobility and vegetation cover in the southwest Kalahari Desert. Earth Surface Processes and Landforms (20): 515-529.

Wiggs, G.F.S, Livinistone, I., Warren, A. 1996 (a). The role of streamline curvature in sand dune dynamics: evidence from field and wind tunnel measurements. Geomorphology (17): 29-46.

Wiggs, G.F.S., Livingstone, I., Thomas, D.S.G., Bullard, J.E. 1996 (b). Airflow and roughness characteristics over partially vegetated linear dunes in the southwest Kalahari Desert. Earth Surface Processes and Landforms 21(1): 19-34.

Wolfe, S.A. 1996. Impact of increased aridity on sand dune activity in the Canadian Prairies. Journal of Arid Environments (36): 421-432.

Yizhaq, H., Ashkenazy, Y., Tsoar, H. 2007. Why do active and stabilized dunes coexist under the same climatic conditions? Physical Review Letters (98): 188001-4.

	Dunefield km²	**Bare Sand km²**	**Beach km²**	**Vegetation km²**	**Deflation km²**
1961	4.42	3.93 **(90%)**	0.26 **(6%)**	0.10 **(2%)**	0.11 **(2%)**
1977	3.70	3.04 **(82%)**	0.18 **(5%)**	0.27 **(7%)**	0.20 **(5%)**
1987	3.63	2.93 **(81%)**	0.27 **(7%)**	0.24 **(7%)**	0.18 **(5%)**
2006	3.67	2.59 **(70%)**	0.40 **(11%)**	0.41 **(11%)**	0.27 **(7%)**

Table 1: Change in the areal extent (km²) for the dunefield, bare sand, beach, vegetation, and deflation surfaces during the years 1961, 1977, 1987, and 2006.

Figure 1: Maspalomas dunefield is located on the southern coast of Gran Canaria, Canary Islands, Spain (A,C). The competent wind regime (i.e. >5.5 ms^{-1}) was recorded at an AEMET meteorological weather station located 0.6 km to the west of Playa de Maspalomas. The wind regime, between 2004-2015, was bi-modal with westerly and easterly wind exceeding threshold values (B).

Figure 2: Maspalomas has experienced widespread urbanization between 1961 (A) and 2006 (C). In 1961 (B), climbing dunes were able to bypass the elevated terrace surface, feeding downwind areas with sediment. Following urbanization or the terrace surface (D), this sediment corridor has been disrupted and continual urbanization has further modified the regional airflow dynamics at the Maspalomas dunefield.

Figure 3: DEM of the Maspalomas dunefield (2006) with the three major phases of construction across the terrace surface including 1977, 1987, and 2006 (A). A castellated mesh was generated with four levels of progressive cell refinement set towards the coupled model surface, maintaining a representative surface gradient of the complex dune topography and urban geometries (B).

Figure 4: Land cover change occurring at Maspalomas for the years 1961 (A), 1977 (B), 1987 (C), and 2006 (D). Changes in the areal extent of the dunefield, urban shadow zone (i.e. $< \delta q'$), acceleration zone (i.e. $> \delta q'$), beach, vegetation, and deflation surfaces have changed through time.

Figure 5: Topographic changes, identified from aerial LiDAR surveys, between the years 2006-2008 (A) and 2008-2011(B). The 2011 LiDAR dataset was unfiltered and vegetation was considered null due to overestimation of the 'bare-earth' surface.

Figure 6: The dune mobility index (M) for the Maspalomas dunefield between the years 1957 to 2011. M values largely remain >200 which are classified as fully active dunes with limited stabilization due to vegetation.

Figure 7: Sediment flux potential (q') during Case 1 and sediment flux perturbation ($\delta q'$)following multiple phases of urbanization for Cases 2-4 (B,C,D).

Figure 8: Surface airflow direction (θ) during Case 1 (A) and airflow direction perturbations ($\Delta\theta$) following multiple phases of urbanization for Cases 2-4 (B,C,D). Arrows indicate the deflection in degrees between the pre-urbanization period (C1) and each subsequent urbanization period (C2,C3,C4).

Figure 9: Surface turbulence intensity (TI) during Case 1 (A) and turbulence intensity perturbations (δTI) following multiple phases of urbanization for Cases 2-4 (B,C,D).

Figure 10: Turbulent flow conditions including counter-rotating vortices represented by surface vectors showing the angle of flow between the streamwise (u) and spanwise (v) flow components (A,B).

Figure 1.

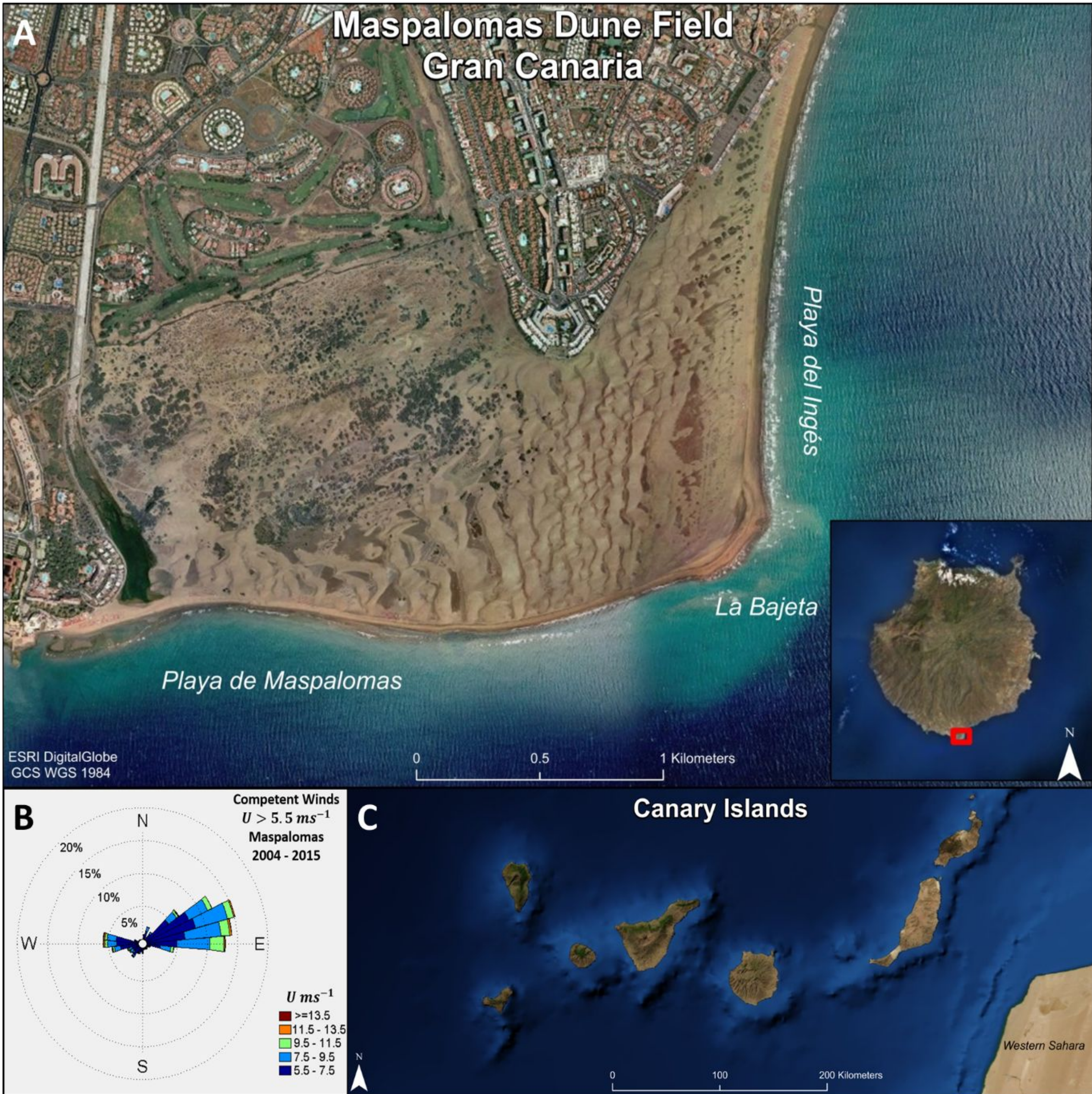
A
Maspalomas Dune Field
Gran Canaria
Playa del Ingés
La Bajeta
Playa de Maspalomas
ESRI DigitalGlobe
GCS WGS 1984
0
0.5
1 Kilometers
N
B
Competent Winds
$U > 5.5\ ms^{-1}$
Maspalomas
2004 - 2015
N
E
S
W
20%
15%
10%
5%
$U\ ms^{-1}$
>=13.5
11.5 - 13.5
9.5 - 11.5
7.5 - 9.5
5.5 - 7.5
C
Canary Islands
Western Sahara
0
100
200 Kilometers
N

Figure 2.

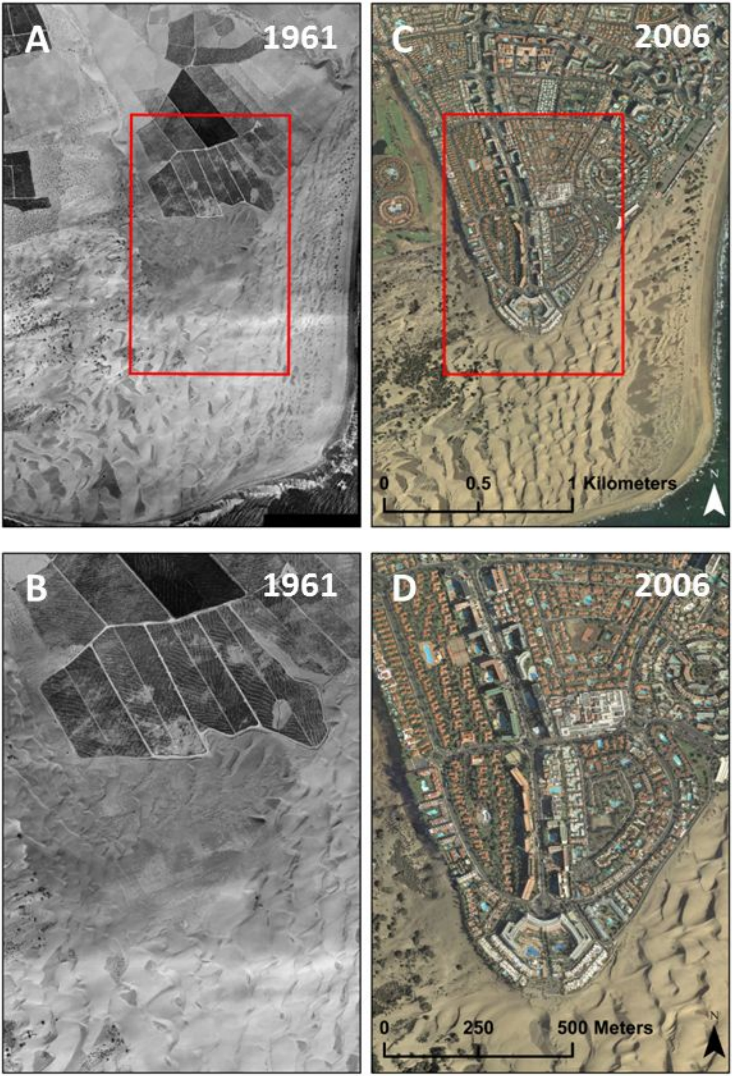

A
1961
C
2006
0
0.5
1 Kilometers
N
B
1961
D
2006
0
250
500 Meters
N

Figure 3.

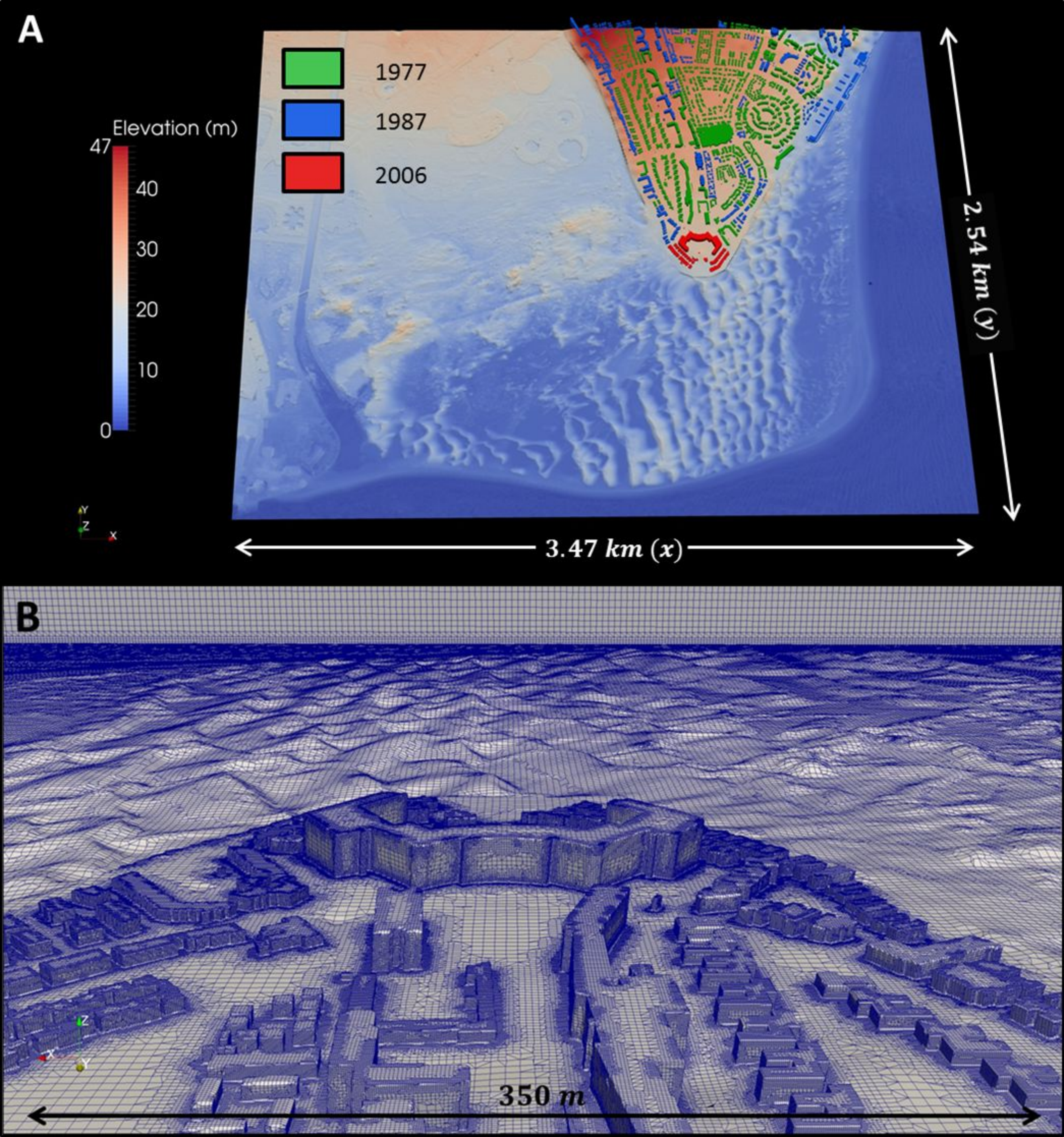
A
1977
1987
2006
Elevation (m)
47
40
30
20
10
0
2.54 km (y)
3.47 km (x)
B
350 m

Figure 4.

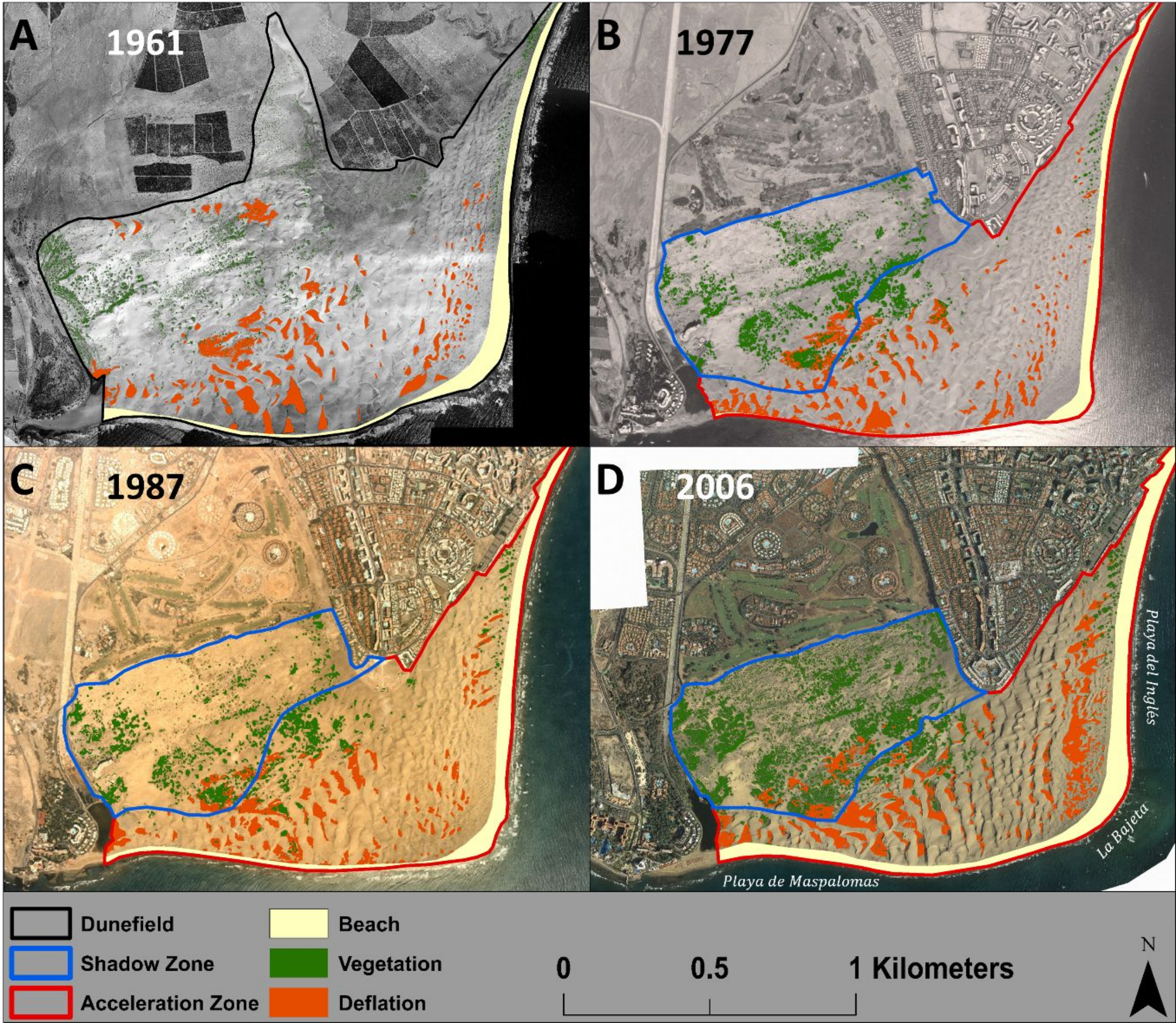
A
1961
B
1977
C
1987
D
2006
Playa del Inglés
La Bajeta
Playa de Maspalomas
Dunefield
Shadow Zone
Acceleration Zone
Beach
Vegetation
Deflation
0
0.5
1 Kilometers
N

Figure 5.

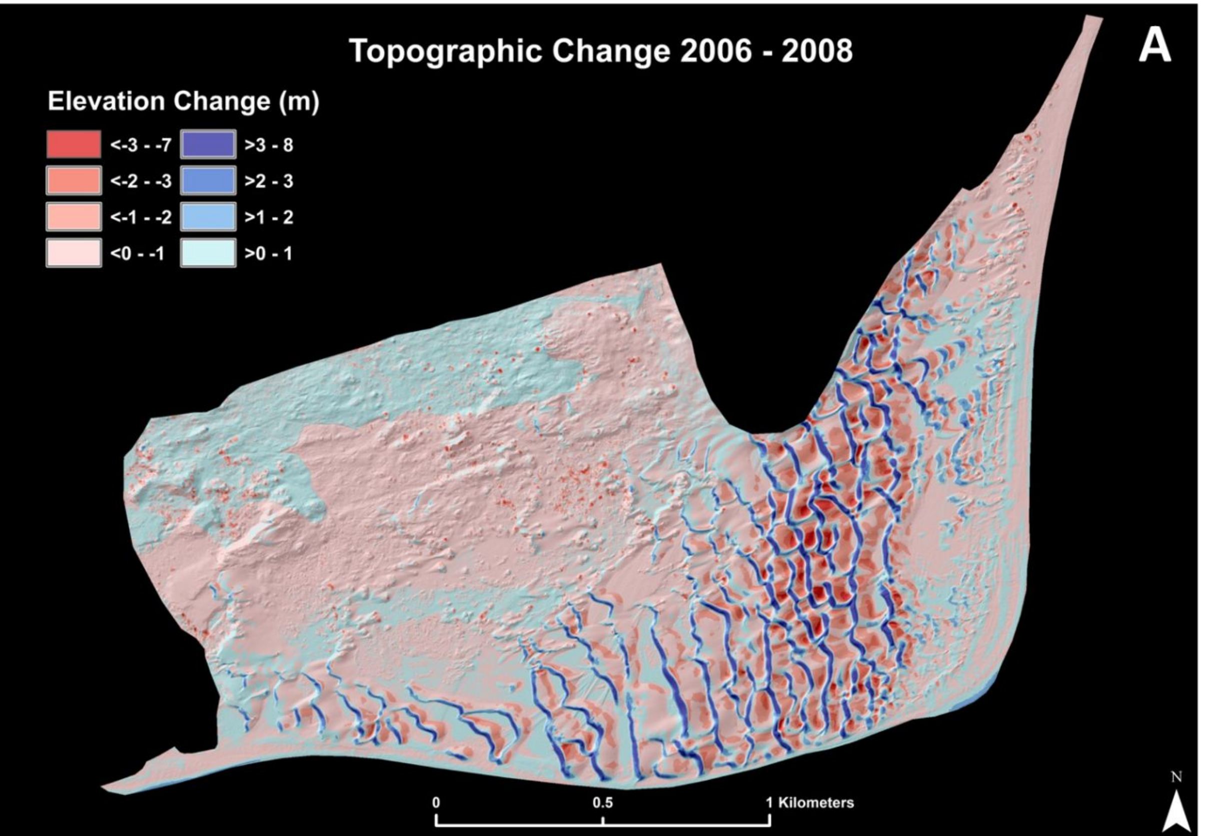

Topographic Change 2006 - 2008
A
Elevation Change (m)
<-3 - -7
>3 - 8
<-2 - -3
>2 - 3
<-1 - -2
>1 - 2
<0 - -1
>0 - 1
0
0.5
1 Kilometers
N

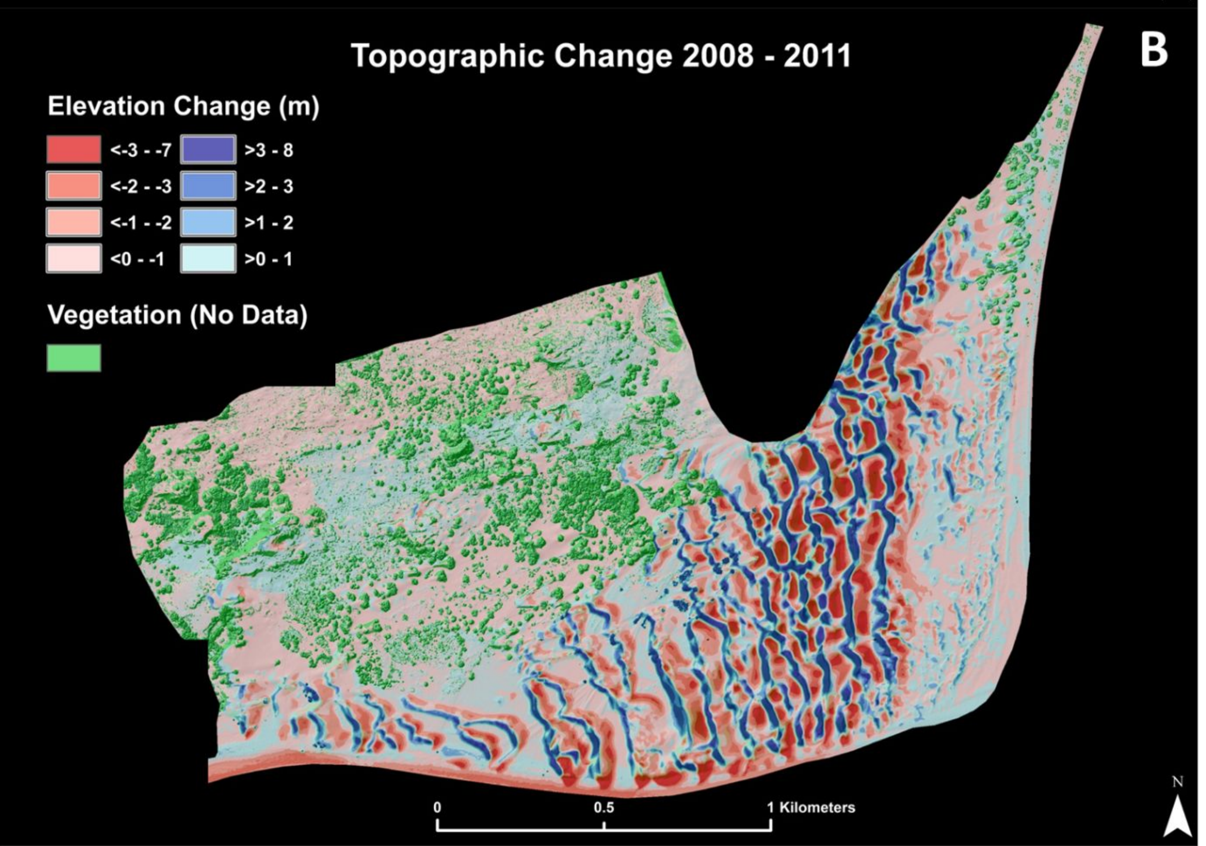

Topographic Change 2008 - 2011
B
Elevation Change (m)
<-3 - -7
>3 - 8
<-2 - -3
>2 - 3
<-1 - -2
>1 - 2
<0 - -1
>0 - 1
Vegetation (No Data)
0
0.5
1 Kilometers
N

Figure 6.

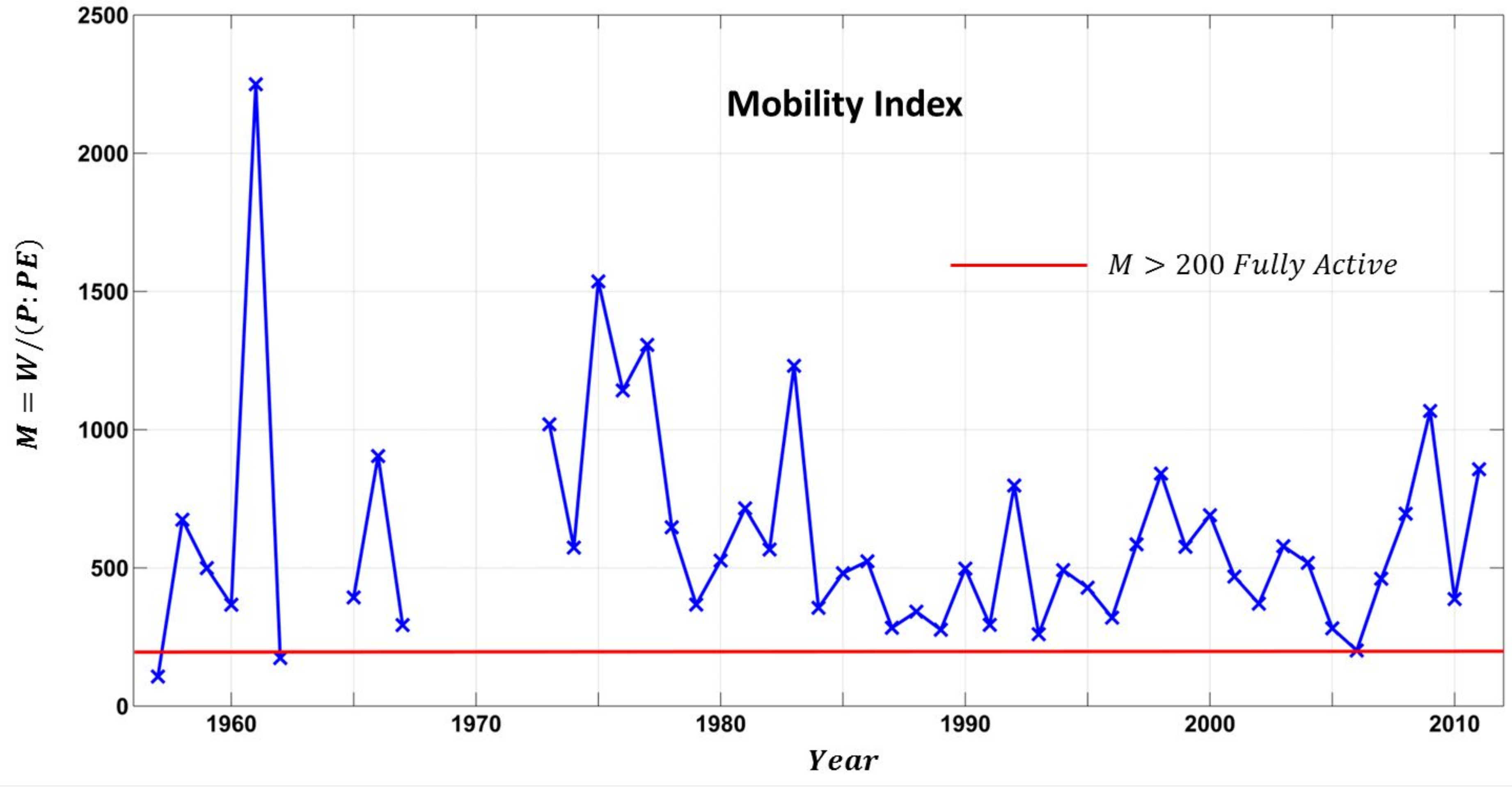

Mobility Index
$M > 200$ Fully Active
$M = W/(P:PE)$
Year
2500
2000
1500
1000
500
0
1960
1970
1980
1990
2000
2010

Figure 7.

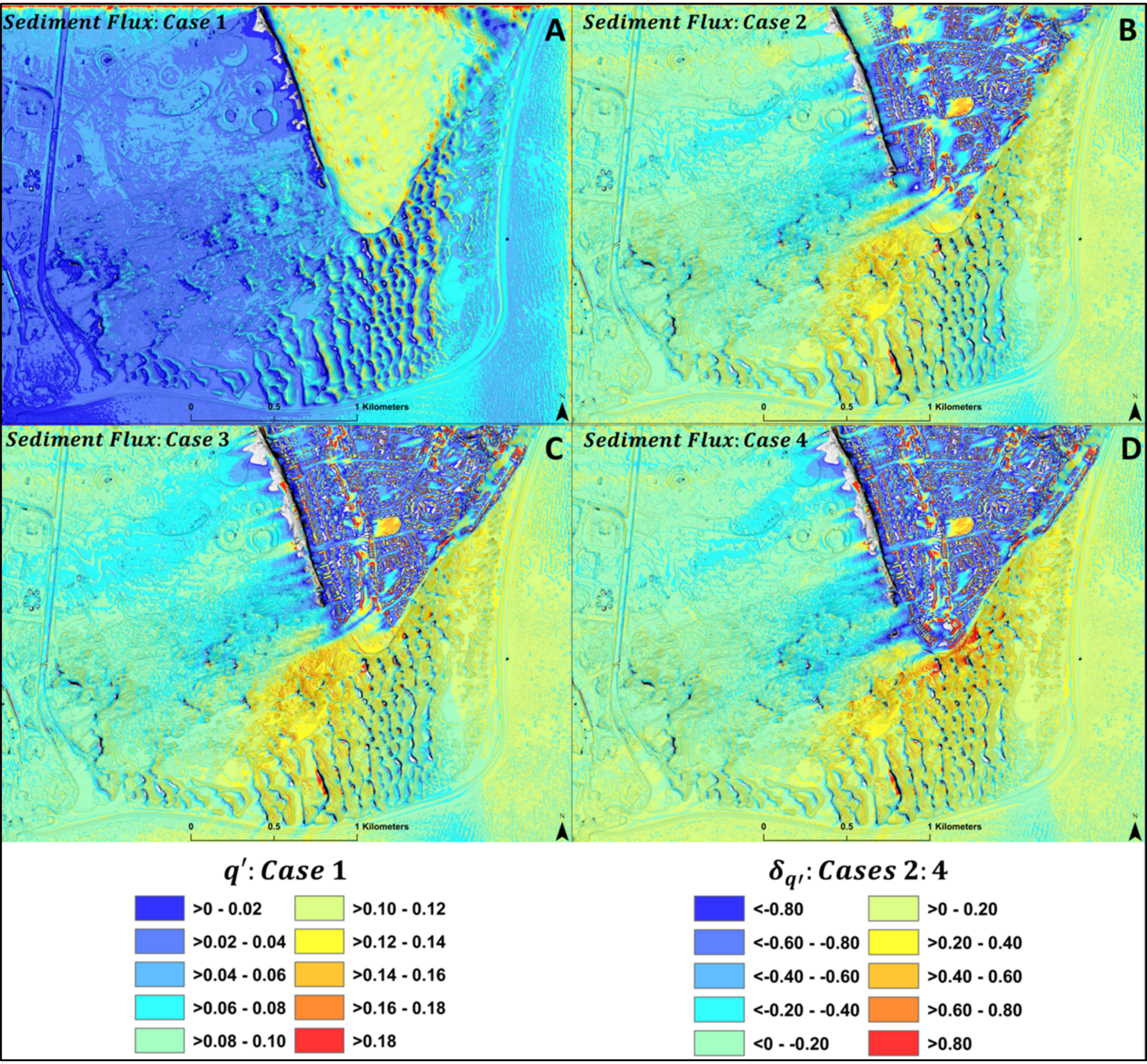

Sediment Flux: Case 1
A
Sediment Flux: Case 2
B
Sediment Flux: Case 3
C
Sediment Flux: Case 4
D
0
0.5
1 Kilometers
N
q': Case 1
>0 - 0.02
>0.02 - 0.04
>0.04 - 0.06
>0.06 - 0.08
>0.08 - 0.10
>0.10 - 0.12
>0.12 - 0.14
>0.14 - 0.16
>0.16 - 0.18
>0.18
δ_q': Cases 2: 4
<-0.80
<-0.60 - -0.80
<-0.40 - -0.60
<-0.20 - -0.40
<0 - -0.20
>0 - 0.20
>0.20 - 0.40
>0.40 - 0.60
>0.60 - 0.80
>0.80

Figure 8.

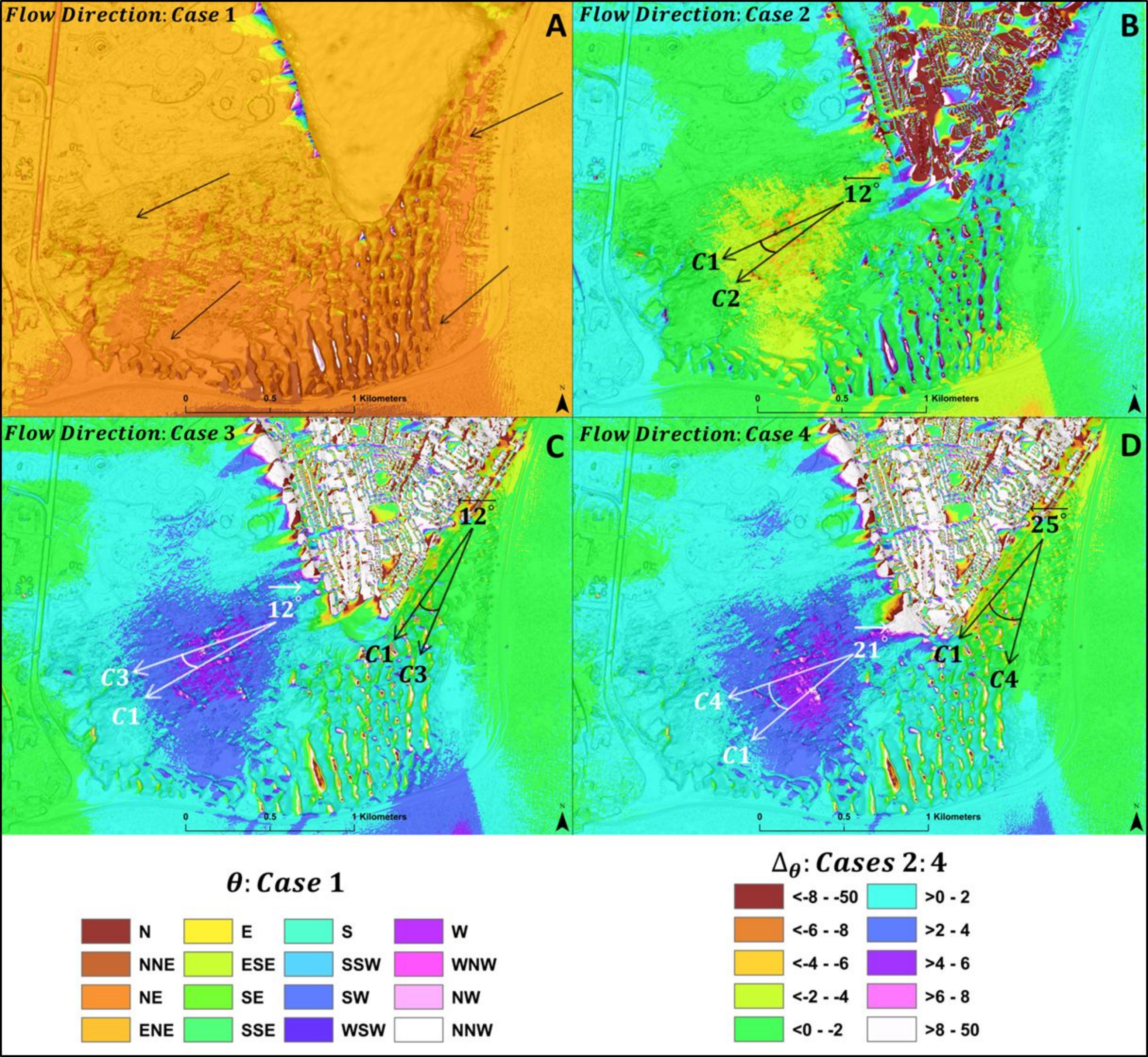
Flow Direction: Case 1
A
Flow Direction: Case 2
B
12°
C1
C2
Flow Direction: Case 3
C
12°
C1
C3
12°
C3
C1
Flow Direction: Case 4
D
25°
C1
C4
21°
C4
C1
0
0.5
1 Kilometers
N
θ: Case 1
N
NNE
NE
ENE
E
ESE
SE
SSE
S
SSW
SW
WSW
W
WNW
NW
NNW
Δθ: Cases 2:4
<-8 - -50
<-6 - -8
<-4 - -6
<-2 - -4
<0 - -2
>0 - 2
>2 - 4
>4 - 6
>6 - 8
>8 - 50

Figure 9.

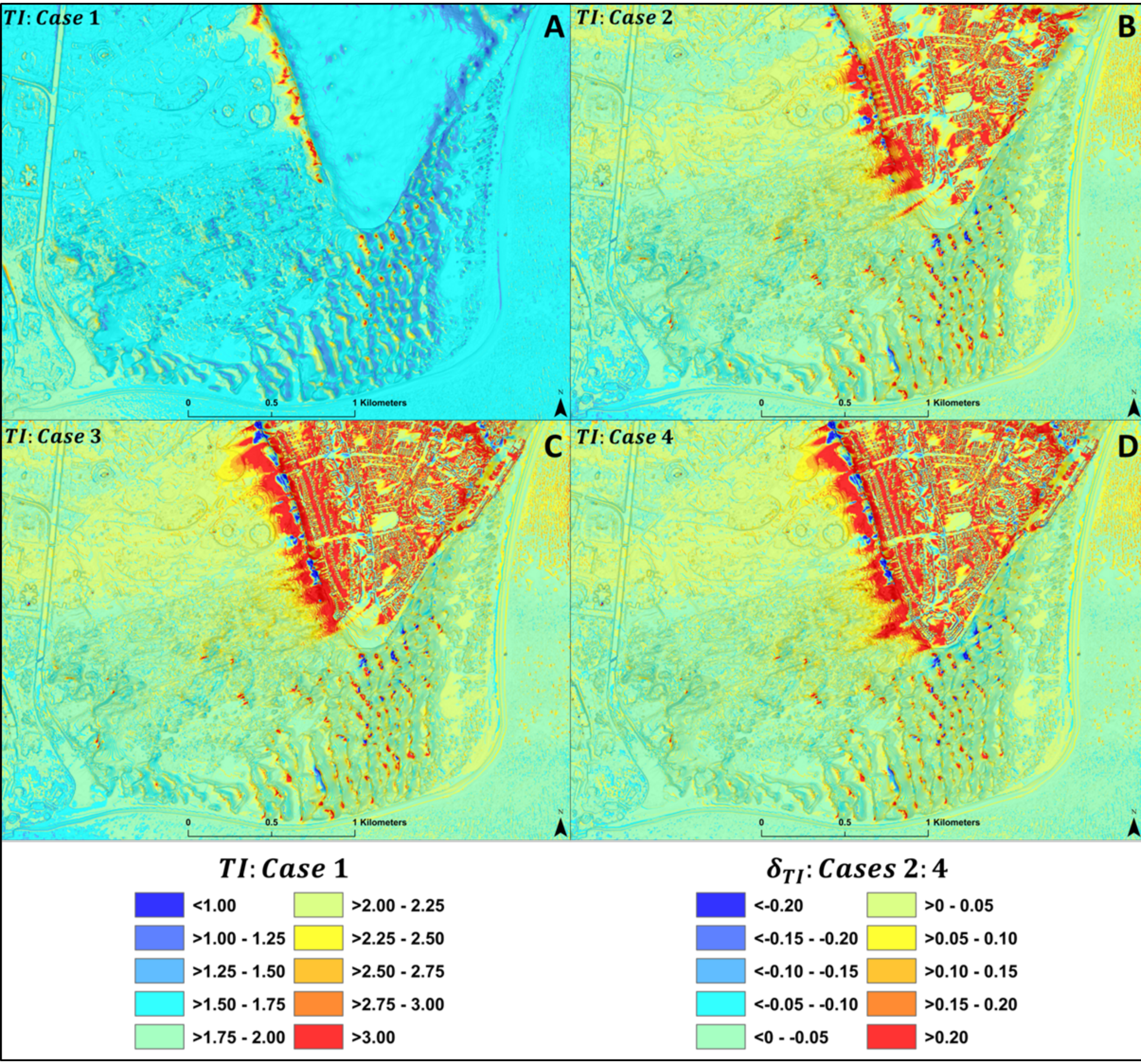

TI: Case 1
A
TI: Case 2
B
TI: Case 3
C
TI: Case 4
D
0
0.5
1 Kilometers
N
TI: Case 1
<1.00
>1.00 - 1.25
>1.25 - 1.50
>1.50 - 1.75
>1.75 - 2.00
>2.00 - 2.25
>2.25 - 2.50
>2.50 - 2.75
>2.75 - 3.00
>3.00
δTI: Cases 2: 4
<-0.20
<-0.15 - -0.20
<-0.10 - -0.15
<-0.05 - -0.10
<0 - -0.05
>0 - 0.05
>0.05 - 0.10
>0.10 - 0.15
>0.15 - 0.20
>0.20

Figure 10.

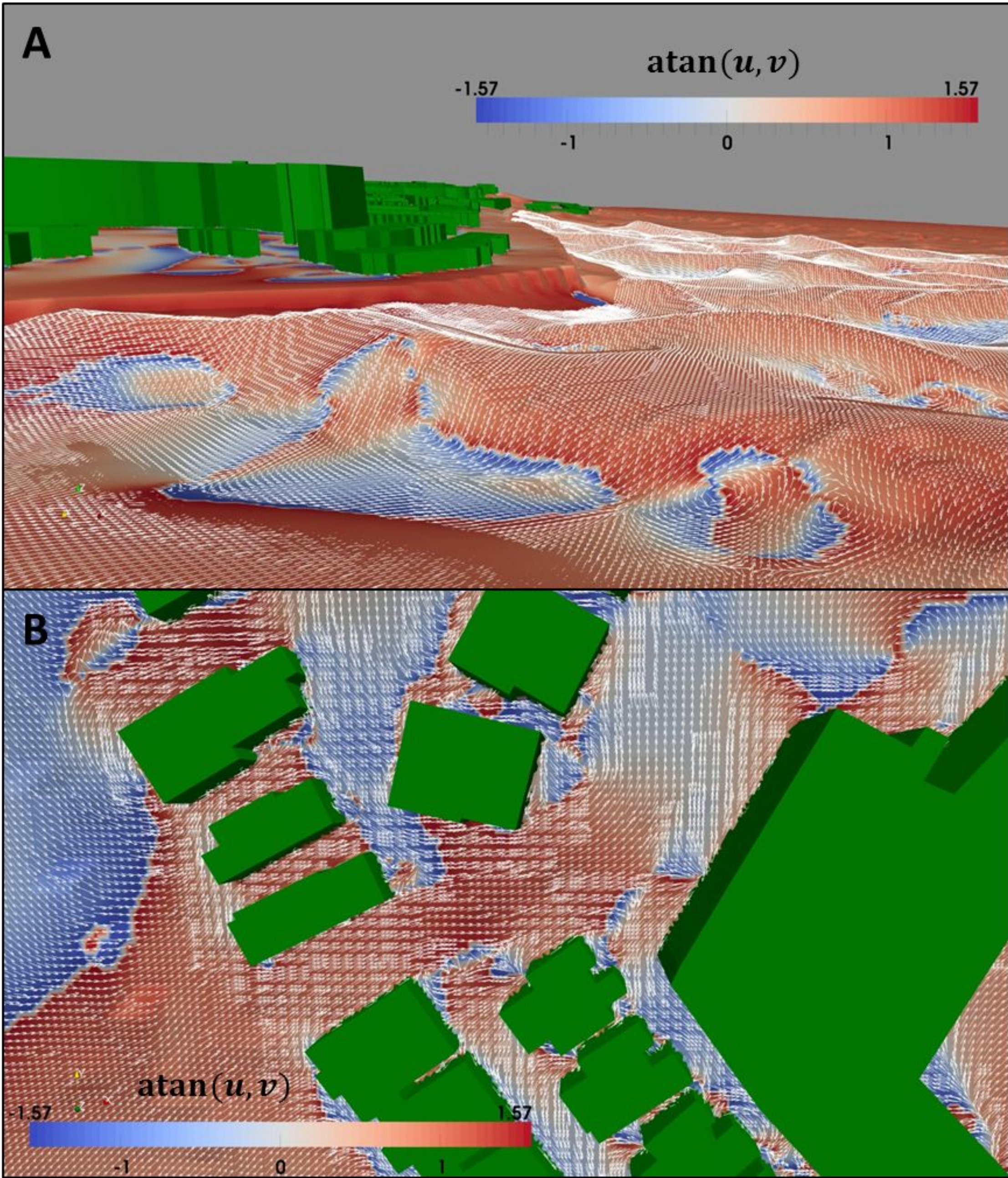
A
atan(u, v)
-1.57
1.57
-1
0
1
B
atan(u, v)
-1.57
1.57
-1
0
1